Experimental and Analytical Assessment of the Influence of Masonry Façade Infills on Seismic Behavior of RC Frame Buildings

Francisco J. Pallarés[1], Antonio Davia[1], Wael M. Hassan[2], Luis Pallarés[1]

[1]*ICITECH, Universitat Politècnica de València, Camino de Vera s/n, 46022 Valencia, Spain*

[2]*Civil Engineering Department, University of Alaska, Anchorage, 3211 Providence Dr., Anchorage, AK 99508, USA*

Corresponding author:

Francisco J. Pallarés
Universitat Politècnica de València,
Camino de Vera s/n, 46022
Valencia, Spain
frapalru@fis.upv.es

ABSTRACT

On May 11, 2011 at 6:47 p.m., an M5.1 earthquake took place in Lorca at a depth of 4 km, in the Region of Murcia, south of Spain, which resulted in nine fatalities and 324 injuries and major built environment damage. Approximately 80% of the residential buildings were affected with various degrees of damage, 5% with severe structural damage and 13% with moderate structural damage, in addition to the damage of infrastructure and public buildings. Reconnaissance and expert analyses revealed that one of the main causes of damage during the Lorca earthquake was the interaction between the non-structural elements and the seismic-resisting framing of the buildings. Studies on this interaction, that started in the 1950s, led to the development of a wide range of macro-models that simulate the stiffness of the masonry infills using one or more equivalent diagonal strut(s). Following an extensive literature review, 12 mathematical expressions have been compiled to estimate the horizontal stiffness of the equivalent strut that simulates the behavior of masonry infills that make up a typical façade of many modern buildings. Two full-scale tests under horizontal cyclic displacement reversals have been carried out on two 5x3m concrete frames: one frame with masonry infill simulating a regular façade; and the other is a bare control frame. The comparison of both tests enabled quantifying the stiffness contribution of the façade infill and identifying the simplified expression that best fits the horizontal stiffness. Using this expression, a realistic seismic design of a prototype building in Lorca, Spain, is conducted under the typical assumption of most modern building codes to consider masonry infills as non-structural elements, and consequently the designed building was seismically assessed considering the influence of the infills. Results of the assessment are in accordance with the real damage patterns observed during the Lorca earthquake reconnaissance.

KEYWORDS: masonry infills; interaction; equivalent strut; concrete frames; macro-modeling; façade; cyclic

1. INTRODUCTION

Every time an earthquake occurs and affects frame buildings with masonry infills, the important role these infills play in the dynamic response of buildings and their dangerous structural interaction become more apparent. Many countries in the Mediterranean area, Latin America and Asia regularly use masonry-infilled frames in construction. Examples of past earthquake damage in this type of construction can be found in FEMA P-774 (2009) [1].

Masonry is an excellent construction material that, due to its characteristics, has a highly complex and variable behavior, especially during earthquakes. Masonry applications are very common in buildings for the construction of partitions, enclosures and walls due to its good thermal, bearing and acoustic characteristics. Masonry infills have traditionally been considered as non-structural elements by engineers and seismic provisions in building codes. However, many studies have shown the great influence they have on seismic loads, such as Smith and Carter (1969) [2] and Bertero and Brokken (1983) [3], that highlighted the increase in structural stiffness and the decrease in the natural period of the building, leading to increased seismic forces (Figure 1). Moreover, Negro and Verzeletti (1996) [4] and Al-Chaar et al. (2002) [5] demonstrated the importance of considering masonry partitions in the dynamic characteristics of buildings, and El-Dakhakhni (2002) [6] concluded that not considering these walls in the seismic design of buildings could threaten structural safety during earthquakes. The major change in global building stiffness due to the presence of masonry partitions was emphasized by Pallarés and Pallarés (2016) [7], which experimentally showed the variation of stiffness in masonry infilled frames during the initial stages of a seismic event. Despite experimental evidence confirming the significant impact of masonry infills on the global building stiffness and its seismic response, and although it has been shown that these infills participate in lateral resistance transmitting additional forces to the structure, the usual practice in building design is to ignore their contributions, considering them as non-structural elements.

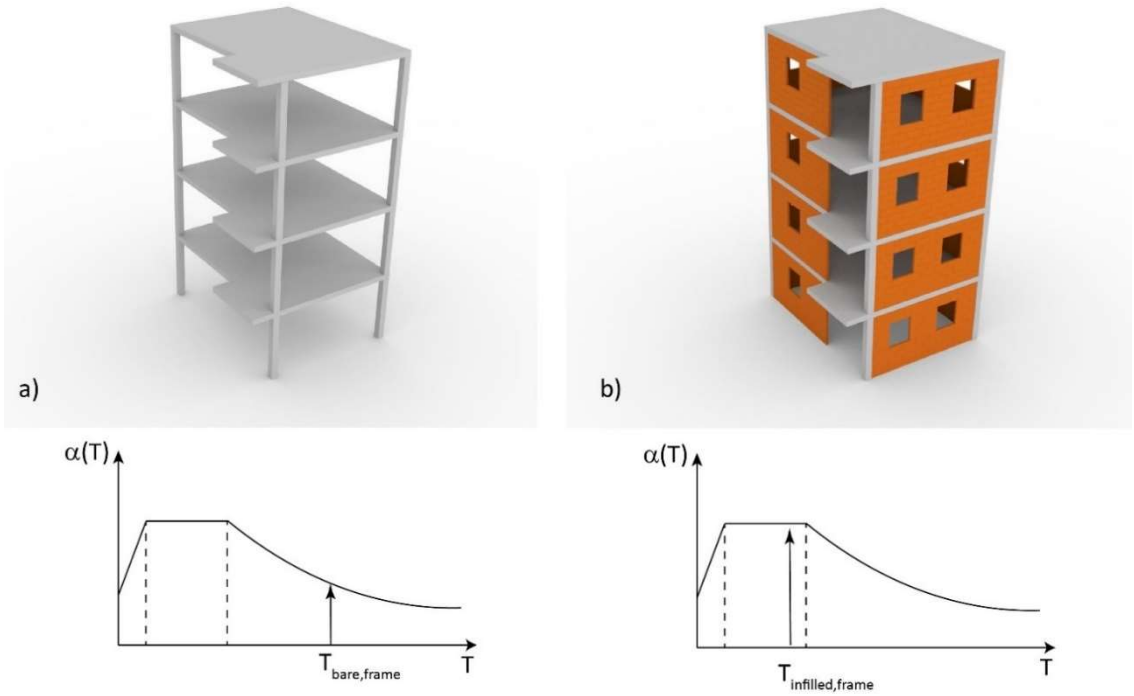

Figure 1: Spectral acceleration. Fundamental periods of the a) numerical model; and b) 'as built' building

When an earthquake strikes, three dimensional (3D) ground shaking is translated into horizontal and vertical displacement demands on buildings. Horizontal seismic forces are concentrated at the floor level, and a practical method to consider the effect of masonry infills in design is to assume the presence of an equivalent diagonal strut, as shown in Figure 2. These struts can be modeled with linear and nonlinear properties to mimic the infill panel behavior. When these horizontal seismic forces are large enough, the diagonal stresses lead to cracks in partitions and joint failure that can result in structural collapse. This effect was evident during many past earthquakes such as Lorca (Spain, 2011) and L'Aquila (Italy, 2009), which can be found in: Ricci et al. (2013) [8], Alarcón and Benito (2014) [9], Gómez (2015) [10], De Luca et al. (2014) [11], Hermanns et al. (2014) [12], Ruiz-Pinilla et al. (2016) [13], and Romão et al. (2013) [14].

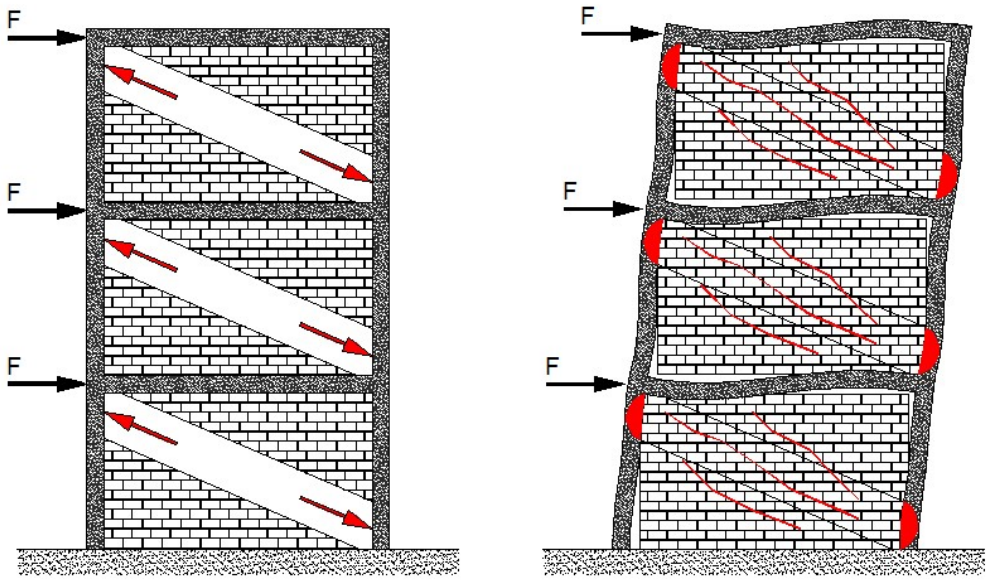

Figure 2: Formation of diagonal strut in the masonry panel under horizontal actions as consequence of in-plane drift effects.

Simulating the effect of masonry infills (partitions and enclosures) in the seismic design of buildings is a complex, yet a necessary issue, in light of the great influence they have on the dynamic response of buildings and their devastating impacts that have been well documented during past earthquakes. Special attention should be paid to the façade panels, since these enclosures are typically very stiff, dominating the initial responses and increasing the seismic demand. There have been many studies to develop numerical models that take into account the influence of masonry infills. They can be used in the usual design of buildings without having to resort to complex calculations, based on developing simplified models that consider the formation of one or more diagonal struts to simulate the panel. A summary of these models can be found in several studies including Liberatore et al. (2018) [15] and Gergis and Hassan (2014) [16], showing that these models can conveniently reproduce test results when properly calibrated. In addition, Sandoli et al. (2020) [17] more recently proposed a formulation for narrow partitions (spandrel), Kareem and Pantò (2019) [18] compared the equivalent diagonal strut model and a two dimensional (2D) discrete macro-model, and Huang and Burton (2019) [19] developed classification models to predict the in-plane failure modes of infill frames based on machine learning techniques.

Many experimental programs were conducted on seismic performance of masonry infilled frames and can be found in literature. Examples of the most recent ones are Yu et al. (2019) [20], where the authors study progressive collapse in RC infilled frames showing brittle shear failure, Stavridis et al. (2012) [21] and Hashemi and Mosalam (2006) [22], who performed tests using shaking table on RC frames infilled with masonry walls, and Costa et al. (2011) [23] and

Markulak et al. (2013) [24] testing autoclaved aerated concrete blocks as infill in masonry walls of buildings, or Zhai et al. (2016) [25]. All of these studies exhibit the continuous research effort put into this interesting and current topic. However, only a few studies can be found dealing with double layered panels representing façade enclosures, such as Palieraki et al. (2018) [26] for Greek buildings or Furtado et al. (2018) for Portuguese buildings [27].

Taking this into consideration, there is a need to provide more design-oriented test data on the seismic performance of masonry infilled façade frames with double infill panel layers, typical in Mediterranean countries, to characterize cyclic response parameters adapted to this typology. Furthermore, diagonal strut macro-models are adjusted to single infill panels test results hence tests are warranted to calibrate the proposed model to double infill layer construction. To this end, to ensure a representative numerical simulation of Lorca 2011 building configuration and realistic earthquake damage prediction using the proposed analytical strut model, experimental tests featuring typical construction practices in the regions are needed.

The main objective of the current study is to experimentally and analytically characterize the influence of masonry infills, especially façade enclosures, on the seismic response of buildings. Another primary objective is to propose a quantitative method to account for the effect of masonry infills in routine seismic design calculations through adopting from existing literature, and modifying as needed, a simplified macro-model that adequately simulates their contribution. To this end, among the simplified diagonal strut models proposed in the literature, the model that best predicted the test results of a full-scale frame with façade masonry infills was adopted in this study and applied to a real case of an actual building in the city of Lorca (Murcia, Spain). Seismic design of the building was performed under the typical hypothesis of considering only the moment frame resistance. Subsequently, the building design was assessed under the hypothesis of including the effect of the façade enclosure using the simplified model proposed. The mathematical strut models have been calibrated based on experimental full-scale tests. The results of the comparison and the conclusions showed good agreement with the reconnaissance observations after the Lorca earthquake proving that damage caused by the Lorca earthquake could have been predicted and avoided in many cases had the effect of the masonry façade infills been considered.

2. EXPERIMENTAL PROGRAM

This section describes the laboratory work carried out and the results observed when comparing the cyclic behavior of a reinforced concrete bare frame and a masonry infilled RC frame with double masonry panel as it is typically constructed in the facades of real buildings. Two full-scale tests have been carried out, described herein:

- Bare Frame. This test specimen is a reinforced concrete bare frame without infill. This frame aims to capture the real response of this type of frame, which is used for modeling purposes in routine seismic design of buildings. Test specimen's details are presented in the next section.

- Infilled frame. This test specimen is a reinforced concrete frame with a conventional façade masonry infill type. This infill is made up of two different layers of perforated clay brick with mortar. The test results of this frame will provide information about the real behavior of the frames in 'as built' buildings, useful for subsequent modeling purposes and comparisons.

2.1. Test specimen design

The frame to be filled with the façade masonry panels is a reinforced concrete frame made up of two columns and two beams as depicted in Figure 3. The frame is 3 m high and 5 m wide and was designed according to the Spanish Standard Seismic Code, NCSE-02. (2002) [28], representing a

low ductility “ordinary” full-scale moment frame located in the upper floors of a mid-rise building up to seven floors designed without considering the effect of infills.

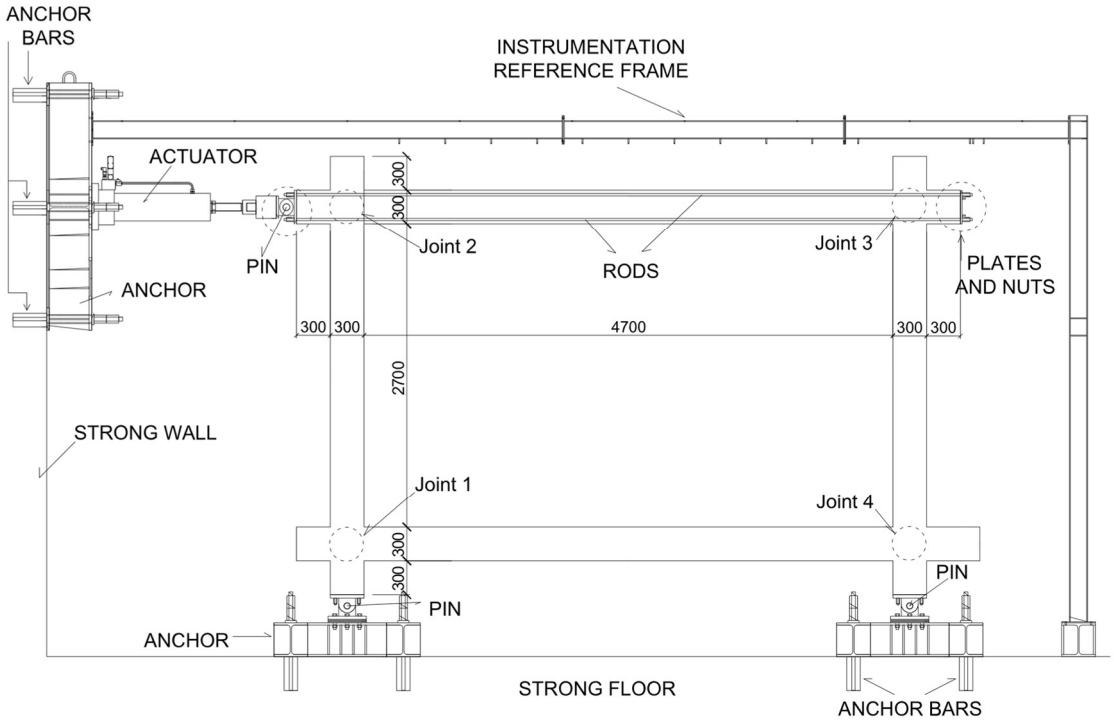

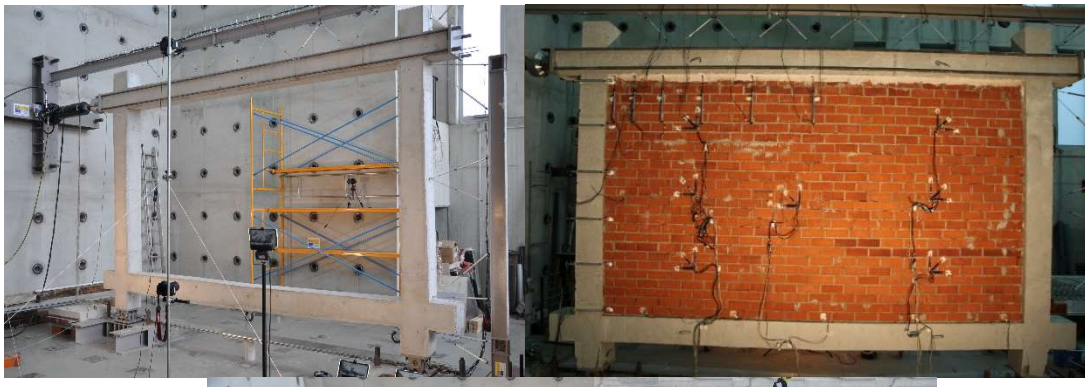

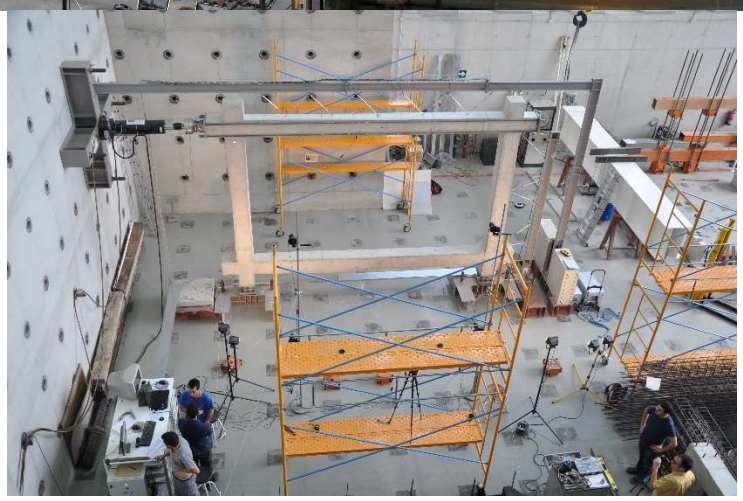

Figure 3. Test layout: test setup (top), bare frame (center left), infilled frame (center right), and general overview of the test rig (bottom)

The cross sections for all concrete elements is 300x300 mm. There is an extension stub of each column and beam beyond the joints to allow for proper anchorage of the reinforcement. The frame is attached to the reaction floor by means of two pin supports at the column bases.

The columns are longitudinally reinforced with (8 Dia. 12) reinforcement bars over the entire length except, approximately, the bottom third, where 6 of these longitudinal reinforcement bars overlap with 15 mm diameter Dywidag bars (Figure 4.a), which are necessary to attach the frame to the laboratory reaction floor. Transversally, the columns have 8 mm hoops every 150 mm (Figure 4.b), except in the area of extension stub under the lower joints, where the hoop spacing is 50 mm. On the other hand, the beam's primary longitudinal reinforcement is (2 Dia. 16) top and bottom along the entire length. At the beam mid-span, the beam has an additional 16 mm bottom longitudinal bar, while in the potential seismic plastic hinge regions near supports, the beam is reinforced with two additional top 16 mm longitudinal bars each side as depicted in Figure 4. The transverse reinforcement of the beam is Dia.6@100mm, and Dia.8@100mm at mid-span and supports, respectively.

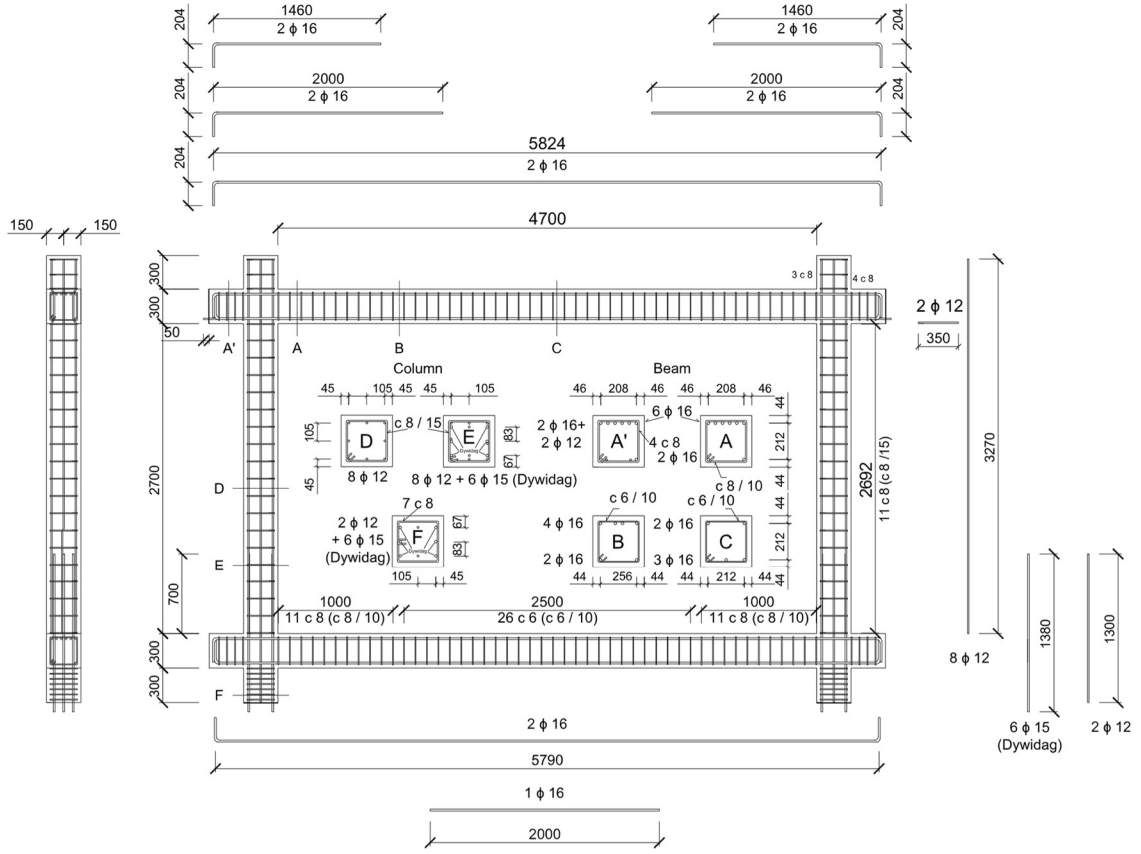

Figure 4. Test specimen reinforcement details.

2.2. Materials

The concrete used to cast the frames was HA-30/F/12/I according to Spanish Standard EHE-08 (2010) [29]. Compression test cylinders of 150x300 mm dimensions were made according to the UNE-EN 12390-1 Standard (2013) [30] for each frame specimen. The mean concrete compressive strengths of the bare frame and infilled frame were 38.2 MPa and 33.6 MPa respectively when tested (elastic modulus E_c=31635 MPa according to Eurocode 2 [39]). The reinforcement steel used was B-500-SD type. Two steel coupons were tested in tension and the actual yield strength was found to be 558 MPa.

The mortar was manufactured from a masonry mortar preparation of common use, type M7.5, and specimens were manufactured to obtain flexural and compressive strengths. Specimen sampling, preparation, curing and testing were carried out in accordance with the provisions of the UNE-EN 1015-11 Standard [31]. Table 1 shows the evolution of the mortar resistance at different ages. The experimental tests on the frames were carried out 10 days after pouring the concrete, when the concrete strength reached the design strength of 30 MPa.

Table 1. Mortar strength for infilled specimen.

	Flexural strength (MPa)		**Compressive strength (MPa)**	
Days	Front layer	Rear layer	Front layer	Rear layer
6	2.00	1.80	6.20	4.00
10	3.00	1.70	9.30	5.50

The façade enclosure is a double-wythe infill wall using two types of bricks. The front panel is built with a perforated clay brick of nominal dimensions 240x120x90 mm (Figure 5.a), while the rear panel is built with a hollow clay brick of nominal dimensions 330x70x160 mm (Figure 5.b).

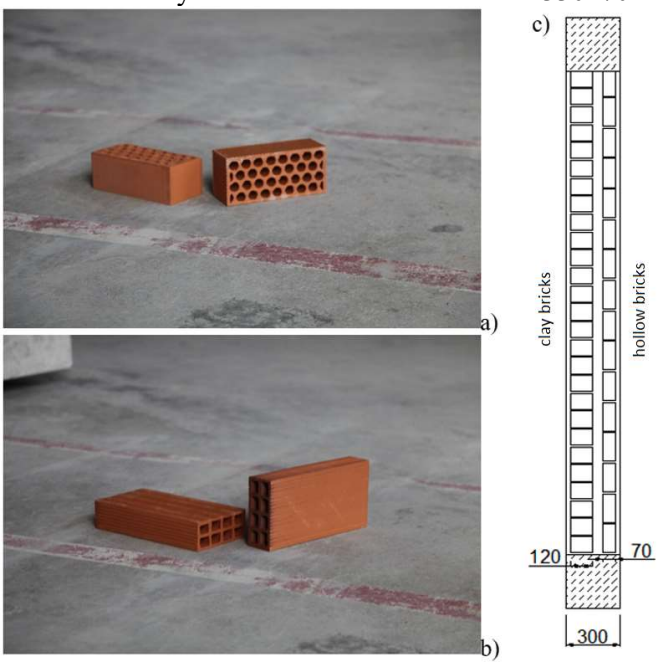

Figure 5. a) Clay masonry units, b) Hollow bricks, c) double-leaf wall in frame

Both brick types have been tested according to the UNE-EN 771-1: 2011 + A1 [32] Standard, both in the direction of gravity loads and in-plane horizontal loads to get the compression strength. Table 2 provides the values for a) the compressive strength (f) of each type of brick in each loading direction, calculated as the average of those obtained in the laboratory, and b) the normalized compressive strength (f_b), which depends on the dimensions of each brick and is calculated according to Annex A of the aforementioned Standard.

Table 2. Compressive strength for bricks

	Clay masonry unit 240x120x90		**Hollow brick 330x70x160**	
	Vertical direction	Horizontal in-plane direction	Vertical direction	Horizontal in-plane direction
f (MPa)	19.4	3.20	4.00	13.2
f_b (MPa)	18.1	2.90	3.10	10.0

2.3. Instrumentation

External instrumentation comprised 300 mm stroke linear variable displacement transducers (LVDT) placed around the specimen perimeter to characterize the deformed shape on of the frame

(Figure 6). The lateral loading actuator has a HBM U10M load cell with a 500 kN load capacity and 250 mm stroke capacity in both tension and compression directions.

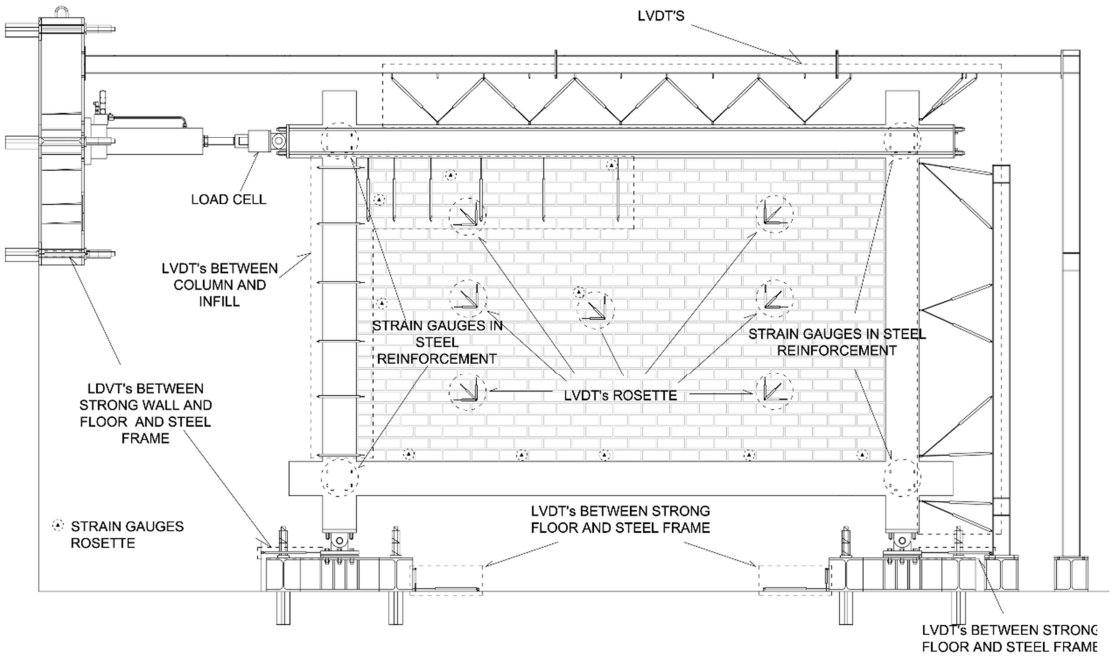

Figure 6. Strain gages and LVDT locations in the reference frame and infill.

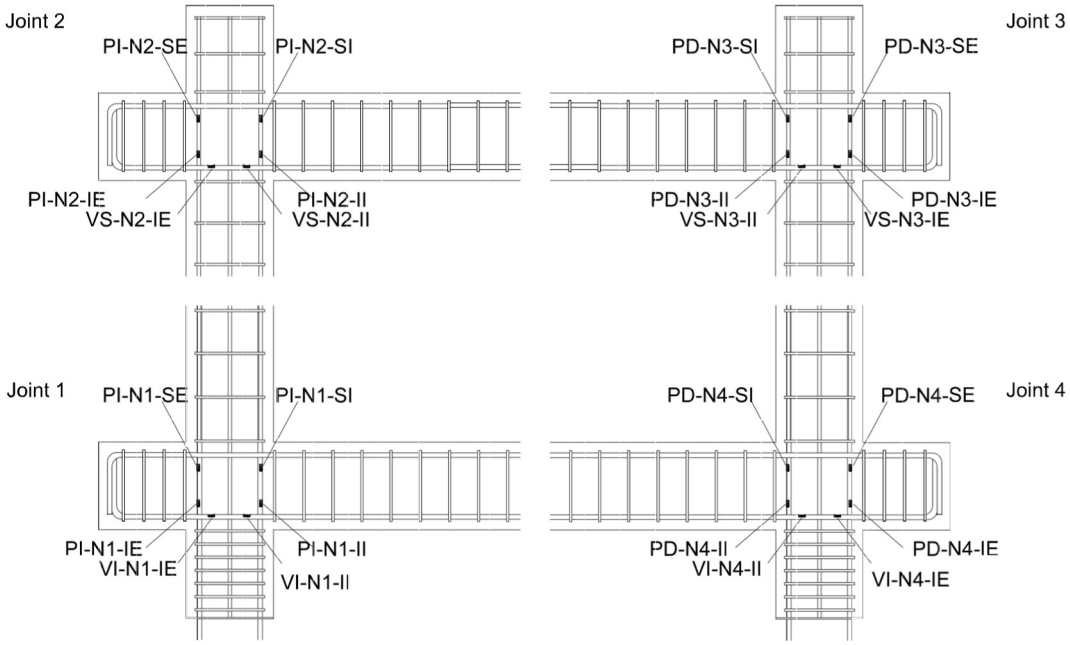

a)

b) 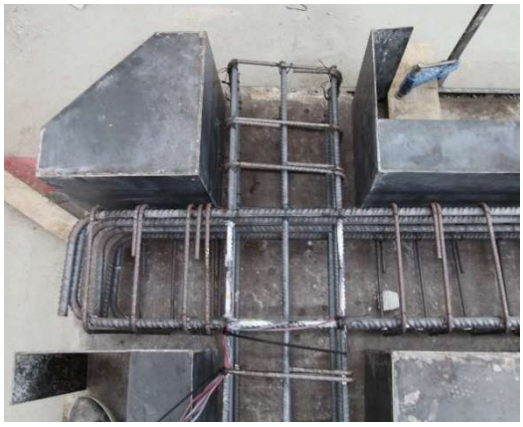

Figure 7. Instrumentation. a) Strain gage layout in joints, b) strain gages in Joint 2 steel cage.

Strain gages were mounted onto longitudinal reinforcement of the frame, specifically in the beam-column joint region to determine steel strains. Figure 7.a indicates the name of each joint and the name of each strain gage inside the joint. Six gages were installed per joint: two gages to the beam's bottom longitudinal reinforcement, two gages to the perimeter reinforcement of the column and the last pair to the intermediate column longitudinal reinforcement (Figure 7.a). Figure 7.b shows Joint 2 with the gages in place.

2.4. Loading protocol

The testing of the frames was conducted under quasi-static horizontal cyclic displacement-controlled reversals applied to the left end of the upper beam. The loading history featured increasing displacement amplitudes (calculated as ratios of the effective yield displacement for each specimen: 0.05, 0.25, 0.5, 0.75, 1, 1.5, 2.25, 3.375, 4, 6, 8, 10, 12, 13), following the loading protocol suggested by FEMA (2007) [33] and presented in Figure 8 for both specimens, in which two cycles are applied for each displacement amplitude. In presenting test results, the positive values represent the push loading direction (loading left to right,) which was the initial direction of loading.

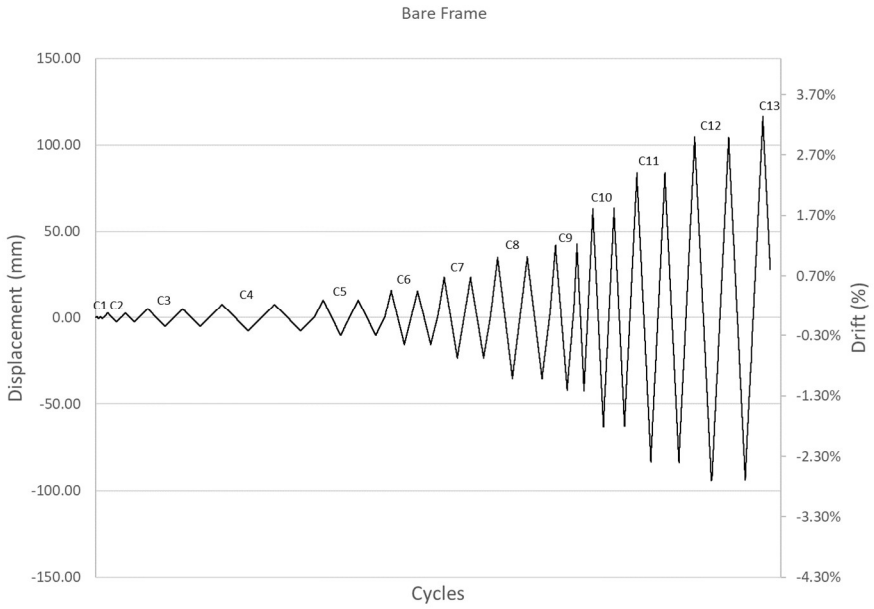

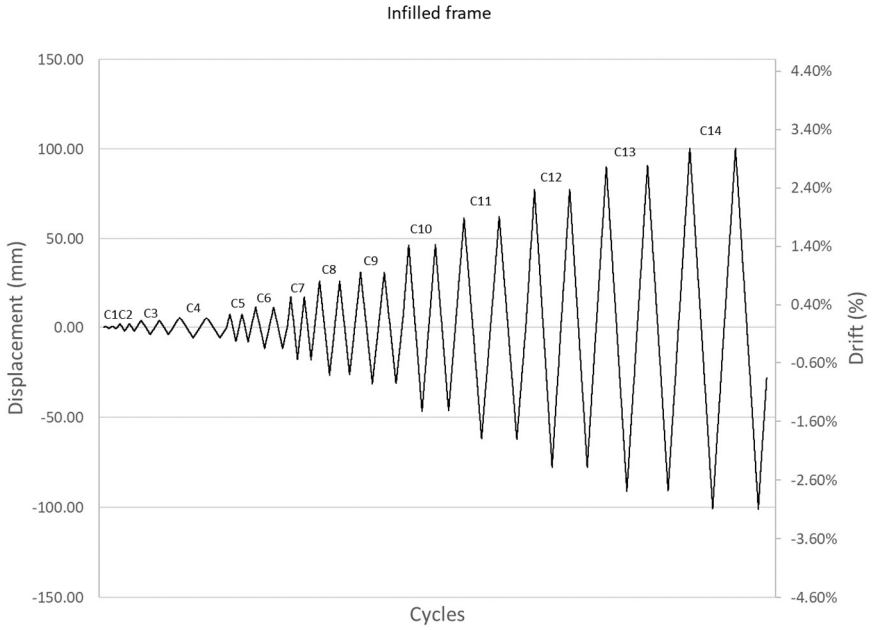

Figure 8. Loading protocol for the two specimens.

3. EXPERIMENTAL RESULTS

3.1. Load-deformation response and stiffness of test specimens

Figure 9 shows the lateral load-deformation hysteresis graphs of the two test specimens. The hysteretic behavior of the bare frame shows much less stiffness and greater linearity with tighter hysteresis loops, while the double-leaf infill frame encloses a larger cyclic loop area, reflecting higher energy dissipation. The initial cycles with small displacement amplitudes are quite linear, but as the cracking of the infill and/or the frame occurs (cycle 4), the nonlinear behavior becomes evident. As expected, infilled frame develops higher cyclic strength, reaching a peak value of 223.0 kN at a displacement of 18 mm (0.32% drift, cycle 7), while the peak strength of the bare frame was 99.6 kN at 116 mm displacement (3.33% drift, cycle 13), with post-yield strain hardening trend. At this point the stiffness of the bare frame was very low; one more only positive cycle (not shown in the plot) was done reaching 100.7 kN at 126 mm (3.62% drift), confirming the peak value at 100 kN, and the test was stopped due to stroke limitations in the pull direction. Thus, the lateral strength of the infilled frame is 2.2 times that of the bare frame. As for the post-peak response, the strength of the infilled frame dropped sharply after the first cracks in the infill, but continued to withstand increasing load until it reached a second force peak at around 174 kN for three consecutive cycles starting at 61 mm, 77 mm and 90 mm displacement (1.58% drift-cycle 11, 2.05% drift-cycle 12 and 2.43% drift-cycle 13, respectively), followed by strength degradation.

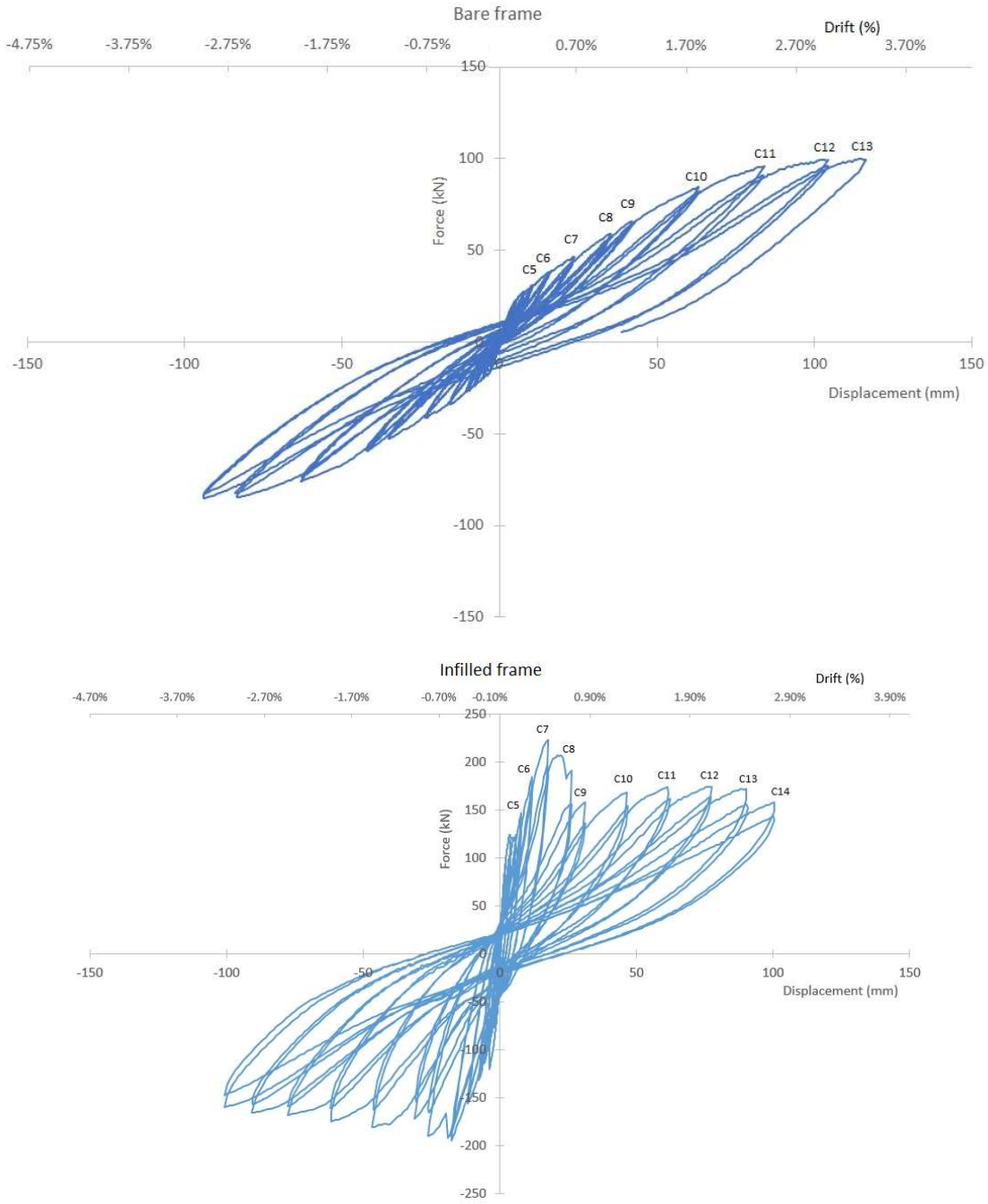

Figure 9. Force, drift and displacement hysteresis responses for bare and infilled frames.

Figure 10 shows the backbone envelope curves of the two test specimens, where the above comments become clearer. The masonry infill started to crack at about 0.1% drift ratio (cycle 4). The infilled frame reached its first peak strength at 0.32% drift (cycle 7), corresponding to masonry infill diagonal strut initial failure. Significant post-peak strength drop of the infilled frame occurred at about 0.76% drift ratio (cycle 9). These relatively smaller drift ratios, concerning seismic performance levels, may suggest that the infill can experience major damage at a "Life-Safe" design-based event. However, the infilled frame maintained its integrity until the "second peak strength" at about 2.43% drift ratio (cycle 13), after which it started to lose its lateral strength. The infilled frame was able to sustain about 2.74% drift ratio (158 kN) suffering about 29% original strength loss and only 9% second peak strength loss. It is noteworthy, however, that the infilled frame strength at 2.74% drift ratio was about 50% higher than that of the bare frame at the same drift ratio. On the other hand, the bare frame has reached its peak flexural strength at

3.33% drift ratio (including strain-hardening and overstrength effects), and experienced no strength loss until about 3.62% drift ratio, when the test was terminated. It is instructive to view these drift capacities in light of performance-based acceptance criteria for modern buildings. As an example, the Tall Building Initiative (TBI 2017) [34], specifies 3% and 4.5% as minimum acceptance drift ratios without significant strength loss for the ground motion suite mean response and for any single ground motion response, respectively. Thus, the bare frame can be considered satisfactory considering these criteria, given its non-deteriorating response until 3.62% drift ratio, while the infilled frame may not be satisfactory despite its higher strength which comes with higher stiffness and lower periods that usually attract higher seismic forces.

Special attention is paid to the stiffness, since it is a key parameter in seismic design and the amount of attracted seismic force. The stiffness of the test specimens is calculated based on the effective secant stiffness of positive and negative displacement cycles combined. As can be seen from the initial slope of the curves, the initial stiffness of the infilled frame is much higher than that of the bare frame, as expected. This can also be observed in Figure 11, where the stiffnesses have been calculated and plotted for each drift cycle. From the first load cycle, the degradation of the stiffness of the infilled frame is very accentuated, decreasing by the 4th cycle to about 37% of the initial stiffness. Three key points can be highlighted in this curve at the 4th, 7th and 9th cycles corresponding to the initial cracking of masonry infill, failure of the diagonal strut and development of secondary struts with slight strain hardening, respectively, as explained in the following sub-section. The initial stiffnesses of the two test specimens are 6.5 kN/mm for bare frame and 50.7 kN/mm for infilled frame (Figure 11). In other words, the initial stiffness of the infilled frame that would be used in elastic calculations in which the effect of the façade partition was considered 8 times higher than that of the bare frame for designs not considering the infills. As the cyclic displacement progresses and the masonry infill degrades, the stiffnesses of both specimens become similar, since the resistant mechanism of the infilled frame becomes the same as that of the bare concrete frame without the contribution of the degraded infill.

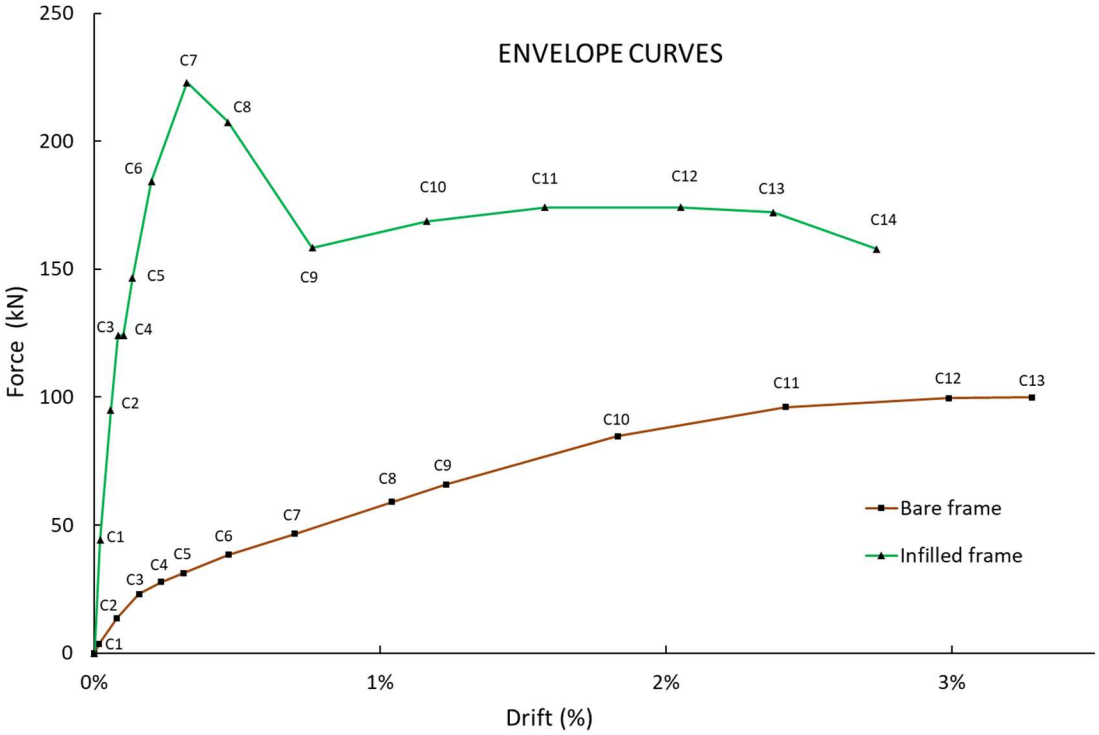

Figure 10. Cyclic backbone envelope curves for test specimens in the push direction

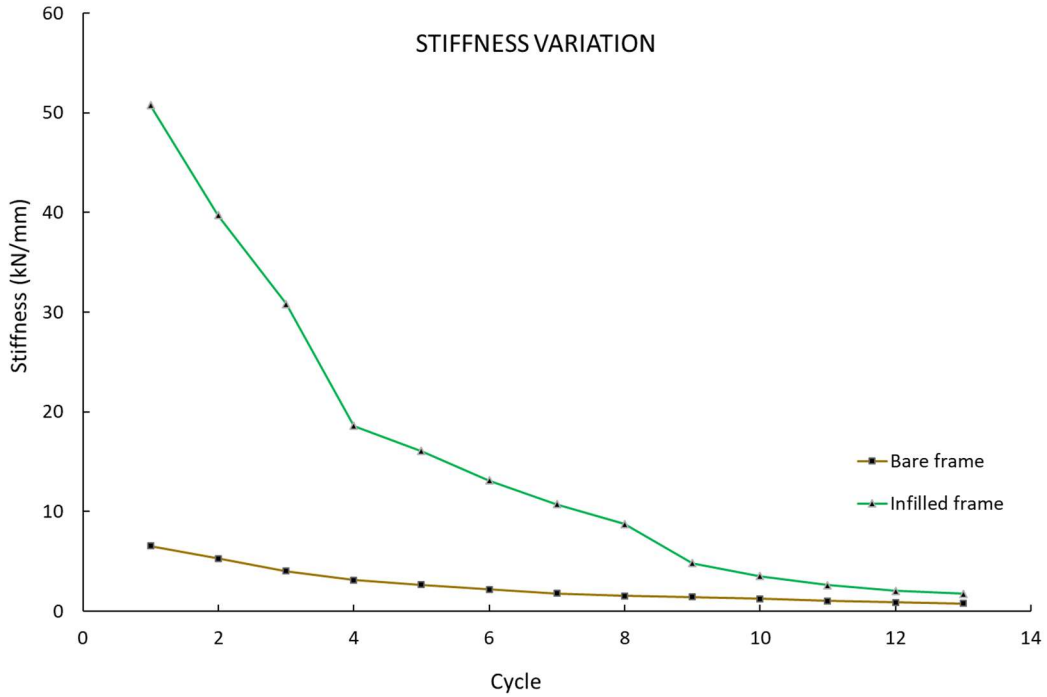

Figure 11. Stiffness variation over loading history of test specimens

3.2. Failure mode

The bare RC frame presents a typical tension-controlled flexural yielding at plastic hinge regions in beams and columns. The upper beam did not experience much cracking and yielding due to axial force exerted by loading actuator, while the lower beam exhibited typical flexural yielding with multiple sizable cracks at the beam-joint interface and along the plastic hinge region as shown in Figure 12. The columns experienced flexural cracking and minor yielding before beam yielding in the case of Joint 2 (upper beam) due to beam axial force, and after beam yielding in case of Joint 1 and 4 as per the design intent of strong-column weak beam scenario. No beam-column joint shear cracking was observed despite the absence of transverse reinforcement. According to Hassan [35], Hassan and Moehle [36], [37], the unconfined joint shear stress demand due to beam yielding may not trigger joint direct shear failure if its lower than the joint shear capacity. In addition, Hassan [35] suggests that the unloaded beam and column stubs, similar to this test configurations, add significant joint shear strength due to concrete confinement effect, which renders the joint in this particular test quite strong, despite no joint hoops were used.

a) 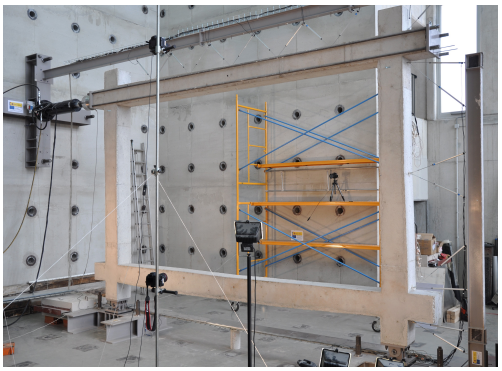 b) 

c)  d) 

Figure 12. Bare frame after test termination (3.62% drift ratio). a) Overall frontal view, b) Joint 1, c) Joint 2, d) Joint 4

As indicated earlier, the behavior in the first cycles was relatively linear, with little energy dissipation per cycle. As the load increased, the backbone envelope curve softened until reaching the peak load of 99.6 kN at 3.33% drift ratio. At this peak load, the yielding of the column longitudinal bar at the joints has already occurred; for instance, column bar strain at Joint 2 was 3.3×10^{-3}, which exceeded the yielding strain (2.79×10^{-3}).

On the other hand, in the test with façade infill, a relatively linear behavior began in the first two cycles, but a short kink at around 124 kN was soon observed as a result of minor infill panel cracking. The concrete cover at the lower column stub extensions was spalled off due to the load transmitted by the Dywidag bars, without further consequences. The stiffness continued to be high in the initial cycles until reaching the peak value of 223 kN at 0.74% drift, when major stepped stair-type cracking of the infill occurred and a sudden decrease in the lateral load capacity took place, which is attributed to initial failure in the diagonal compression strut at this drift level. Subsequently, the stiffness decreased abruptly and the energy dissipated in each cycle increased, accompanied by a new increase in the lateral load capacity due to the development of secondary struts and deployment of the full flexural capacity of the concrete frame, leading to a second peak force at 174 kN at a displacement of 61.4 mm (1.58% drift), which was sustained until 90 mm (2.43% drift). Finally, the degradation of the infill and the frame continued with moderate strength deterioration until the end of the test, where the compression failure of the masonry infill can be observed at the corner of Joint 3 (Figure 13.a) as well as shear cracks (Figure 13.b, 13.c, 13.d) in the beams and columns that give continuity to the cracks in the infill. The shear cracks of the framing elements occurred at the end of "contact regions" which represent the regions of the beams and columns where masonry infill keeps full bearing contact during cyclic loading, and are used to estimate compression strut dimensions. The length of contact regions renders the remainder of column height or beam span shorter and creates a captive column scenario which leads to shear cracking rather than flexural cracking; Gergis and Hassan [16] offers more discussion on contact length modeling. However, the overall behavior of the infilled frame following the first peak can still be considered relatively ductile, despite the shear and compression cracking, due to frame flexural action and the overall systemic interaction between the frame and the infill, which dissipates cyclic energy across several mechanisms.

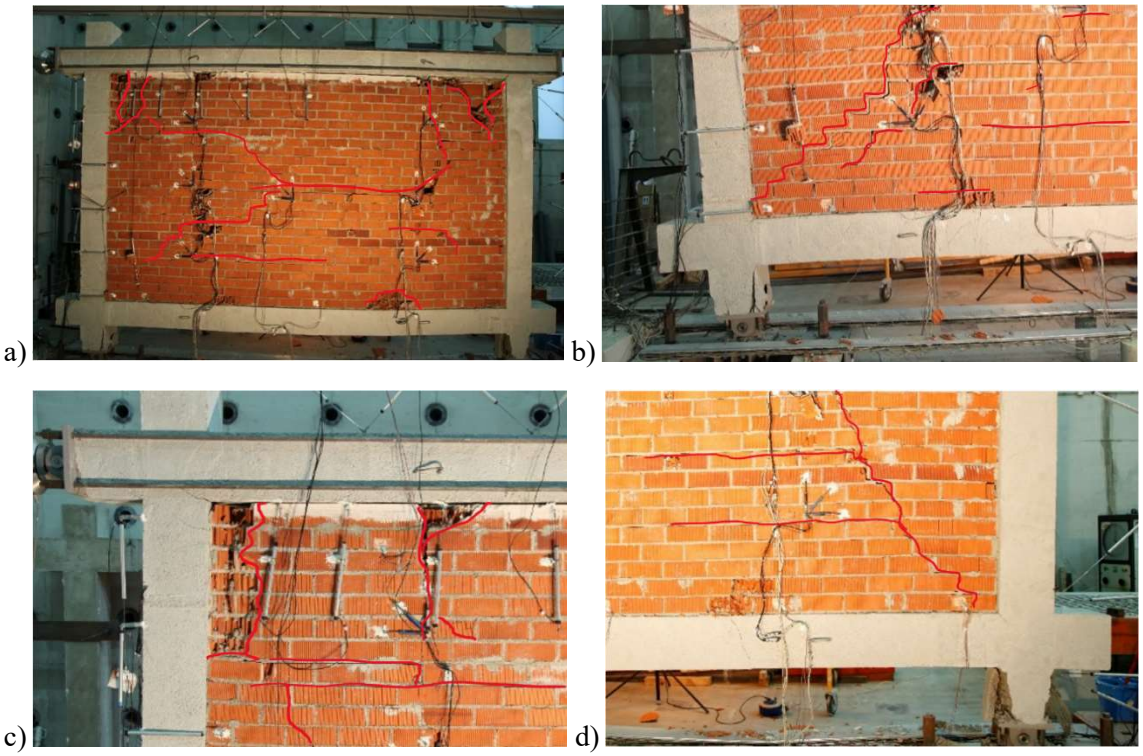

Figure 13. Infilled frame at failure (2.74% drift ratio). a) Overall frontal view, b) Joint 1, c) Joint 2, d) Joint 4

Regarding the strains, Joint 2 is once again the one that exhibits the largest strain in columns reinforcement, reaching a $4x10^{-3}$which confirms flexural yielding of columns. The beam and column flexural sequence of yielding was column at Joint 2, column at Joint 3, then beam at Joint 3.

In summary, the test with a bare frame has a mode of failure due to yielding of the framing elements' longitudinal reinforcement and flexural cracking forming plastic hinges, while the masonry infilled frame with a façade partition has an initial behavior as shear wall failing due to the degradation of the infill in its first stages with cracks compatible with the presence of diagonal compression struts together with shear and flexural cracks in beams and columns, evolving with increasing cyclic drift amplitudes into a failure mode similar to the one observed in the bare frame, showing higher residual strength due to the contribution of secondary diagonal struts.

4. CHOICE OF MACRO-MODEL

The modeling of both the bare frame and the infilled frame with the equivalent diagonal struts is carried out using the SAP2000 software (CSI [38]), which allows the design of structures using the finite element method considering material nonlinearities and geometrical nonlinear analysis, both static and dynamic.

4.1. Bare frame model

Aiming to reproduce the initial stiffness of the structure, the model used is illustrated in Figure 14, which consists of a simple rigid frame 5 m wide and 3 m high, with 0.45 m stub extensions from the ends of each beam and column. The concrete used has a compressive strength equal to that obtained in the control tests ($f_{cm} = 38.2\ MPa$). The value of the modulus of elasticity is obtained as suggested by Eurocode 2 [39] as:

$$E_c = 22000 \cdot \left(\frac{f_{cm}}{10}\right)^{0.3} \qquad E_{cm} = 32800\ MPa$$

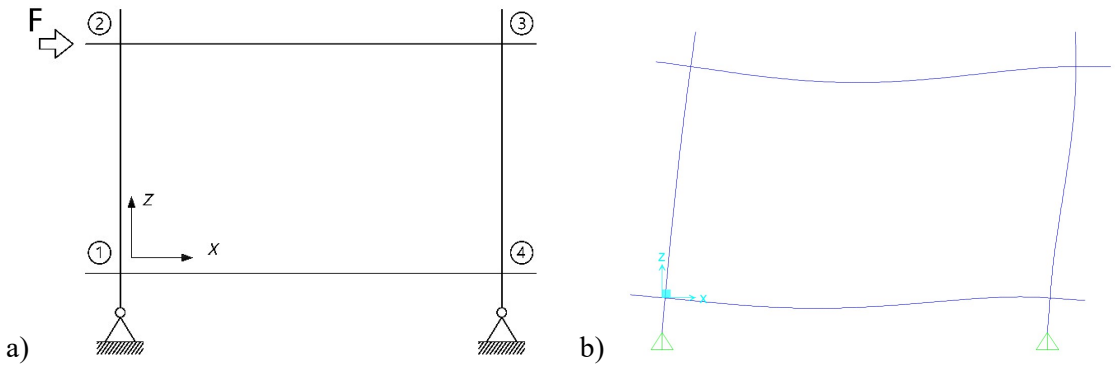

Figure 14. a) Macro-model in SAP2000 for bare frame. b) Deformed shape for the first cycle

A modulus of elasticity of 200 GPa and a yield strength of 500 MPa are assigned to the reinforcing steel. The frame sections are introduced in the structural software according to Figure 4. The columns lower joints are restrained for horizontal and vertical displacements to model the hinge in the supports. Using the structure's self-weight and the horizontal force for the first displacement amplitude, 3.53 kN, the model is solved conducting an elastic analysis to check the stiffness of the structure. A displacement of 0.533 mm (Figure 14f.b) is obtained, which is almost equal to test displacement counterpart, with a negligible error of 3.9% (while the stiffness error was 1.9%). Thus, this modeling was the basis for the subsequent infilled frame model.

4.2. Model of the masonry infilled frame

To model the stiffness of the test infilled frame, this integrated macro-model corresponds to the model designed for the bare frame combined with a diagonal strut pinned to Joints 2 and 4 representing the masonry infill (Figure 15). In the SAP2000 program, this diagonal strut has been represented by a translational spring. Having in mind the skepticism of structural engineers about the difficulty of including the effect of masonry infill in routine seismic analysis and design, this simple model used was to introduce a practical means that can be easily incorporated into the seismic design of buildings that practitioners routinely perform on a daily basis.

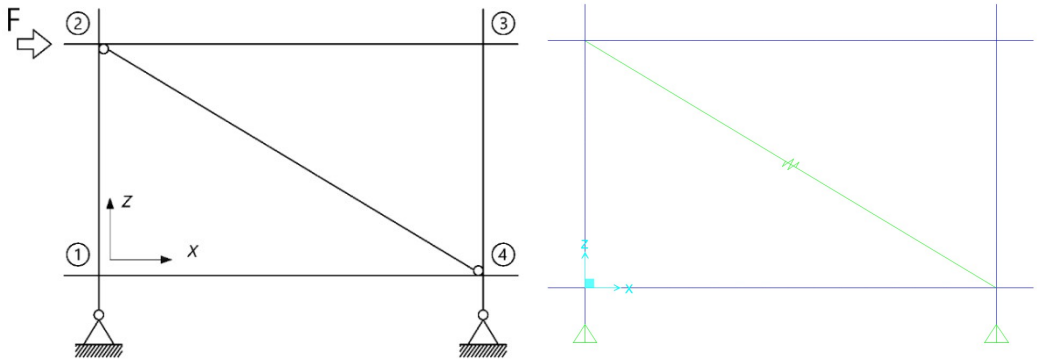

Figure 15. Macro-model in SAP2000 for infilled frame.

The compression strength of the concrete for the infilled frame is different from that of the bare frame, so this value and the modulus of elasticity are modified according to the expression of

Eurocode 2 [39]. In addition, the 4.95 kN/m weight of the masonry is added as an evenly distributed load on the lower beam. To obtain the stiffness of the spring that represents the masonry infill, the actuator force obtained in the test for the first cycle is used, and an approximate value of the stiffness for the diagonal strut is obtained. The frame is analyzed elastically under the concrete's self-weight, the weight of the infill and the actuator force, and it is checked whether the displacement obtained at the point where the force is applied coincides with that recorded in the test. If it does not match, the value of the spring stiffness is modified and, through iterations, the necessary stiffness to represent the actual test is reached. This is the value named k_{strut} , which was determined to be 126,400 kN/m.

4.3. Selected existing equivalent strut models

In this section, the calculation of the stiffness provided by the façade infill is calculated according to different existing models in the literature. The length of the diagonal strut for a single infill layer is controlled by the frame geometry, while its depth is equal to the depth of that infill layer. Thus, only the strut width needs to be determined. Table 3 lists 12 mathematical models for compression diagonal strut width given by different authors and building codes and regulations. They are compared in the present paper to choose the best fitting model to simulate the experimental tests and will be used in the seismic assessment of a real building subsequently.

Table 3. Proposals for strut width

Author or Standard	Equivalent strut width and/or infill's Young's modulus	
Holmes [40]	$w = \frac{1}{3}d$	
Mainstone [41]	$w = 0.175\ \lambda_h{}^{-0,4} d$	
Liauw and Kwan [42]	$w = \frac{0.95\sin(2\theta)}{2\sqrt{\lambda_h}} d$	
Decanini and Fantin [43]	Uncracked infill	$w = \begin{cases} \left(\frac{0.748}{\lambda_h} + 0.085\right) d & si\ \lambda_h \leq 7.85 \\ \left(\frac{0.393}{\lambda_h} + 0.130\right) d & si\ \lambda_h > 7.85 \end{cases}$
	Cracked infill	$w = \begin{cases} \left(\frac{0.707}{\lambda_h} + 0.010\right) d & si\ \lambda_h \leq 7.85 \\ \left(\frac{0.470}{\lambda_h} + 0.040\right) d & si\ \lambda_h > 7.85 \end{cases}$
Paulay and Priestley [44]	$w = \frac{1}{4}d$	
Durrani and Luo [45]	$w = \gamma \sin(2\theta)\, d$ $\gamma = 0.32\sqrt{\sin(2\theta)} \left(\frac{H'^4 E_w t_w}{m E_c I_c H}\right)^{-0.1}$ $m = 6\left(1 + \frac{6E_v I_v H'}{\pi E_c I_c L'}\right)$	
ASCE/SEI 41-06 [46]	$E_w = 550\ f_k$ $w = 0.175\ \lambda_h{}^{-0.4} d$	

TMS [47]	$E_w = 700\, f_k \;\; for\ clay\ bricks$ $E_w = 900\, f_k \;\; for\ concrete\ bricks; w = \frac{0.3}{\lambda \cos\theta}$
CCMPA [48]	$E_w = 850\, f_k$ $w \leq \begin{cases} w_e/2 \\ d/4 \end{cases} \qquad w_e = \sqrt{\alpha_h^2 + \alpha_L^2}$ $\alpha_h = \frac{\pi}{2} \sqrt[4]{\frac{4E_c I_c H}{E_w t_w \sin 2\theta}} \qquad \alpha_L = \pi \sqrt[4]{\frac{4E_c I_v H}{E_w t_w \sin 2\theta}}$
TEC [49]	$E_w = 200\, f_k$ $w = 0.175\, \lambda_h{}^{-0.4} d$
Turgay et al. [50]	$E_w = 850\, f_k$ $w = 0.18\, \lambda_h{}^{-0.25} d$

As the infilled frame used in the experimental phase had two brick layers, first the stiffness of the equivalent diagonal strut representing the front layer is calculated, and later the stiffness of the diagonal strut of the rear layer using the same procedure. Since both struts work in parallel, their stiffnesses are added to obtain the total stiffness of the infill panel.

The input data for this calculation regarding the front and rear layers are listed in Table 4.a and Table 4.b, respectively, while and explanation for the main parameters is found in Figure 16.

Table 4.a. Front infill panel layer data

Geometric data			
$L'\,(m)$	5	$L\,(m)$	4.7
$H'\,(m)$	3	$H\,(m)$	2.7
$h_c\,(m)$	0.3	$b_c\,(m)$	0.3
$h_v\,(m)$	0.3	$b_v\,(m)$	0.3
$I_c\,(m^4)$	0.000675	$I_v\,(m^4)$	0.000675
$t_w\,(m)$	0.12		
Mechanical properties			
$f_b\,(MPa)$	18.10	$f_m\,(MPa)$	9.3

Table 4.b. Rear infill panel layer data

Geometric data			
$L'\,(m)$	5	$L\,(m)$	4.7
$H'\,(m)$	3	$H\,(m)$	2.7
$h_c\,(m)$	0.3	$b_c\,(m)$	0.3
$h_v\,(m)$	0.3	$b_v\,(m)$	0.3
$I_c\,(m^4)$	0.000675	$I_v\,(m^4)$	0.000675
$t_w\,(m)$	0.07		
Mechanical properties			
$f_b\,(MPa)$	3.1	$f_m\,(MPa)$	5.5

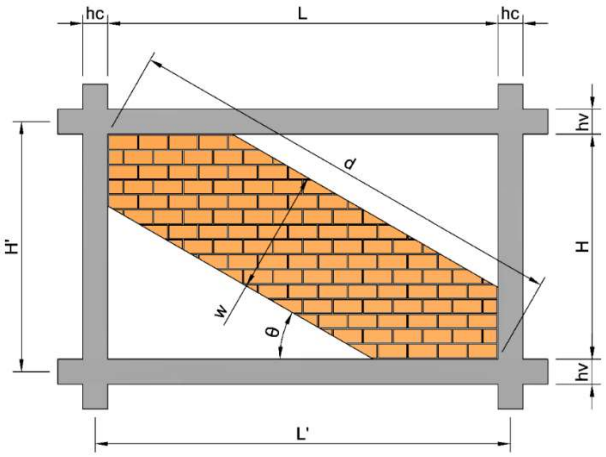

Figure 16. Parameters used in equivalent strut width calculations

This data allows the calculation of the equivalent diagonal strut width and the modulus of elasticity of the infill panel according to the existing literature models, and are collected in Table 5 for each of the two layers combined with the total stiffness.

Table 5. Strut width, Young's modulus and stiffness for the strut models

	Front layer			Rear layer			Global stiffness
	w (m)	E (MPa)	k (kN/m)	w (m)	E (MPa)	k (kN/m)	k (kN/m)
Holmes [40]	1.81	5190	195486	1.81	1272	29266	224752
Mainstone [41]	0.57	5190	61129.0	0.68	1272	11065	72195.0
Liauw and Kwan [42]	1.16	5190	125918	1.48	1272	23902	149820
Decanini and Fantin S. F. [43]	1.57	5190	169957	2.25	1272	36370	206327
Decanini and Fantin C. F. [43]	1.10	5190	119389	1.74	1272	28201	147590
Paulay and Priestley [44]	1.36	5190	146615	1.36	1272	21949	168564
Durrani and Luo [45]	0.92	5190	99411.0	1.11	1272	17995	117406
ASCE/SEI 41-06 [46]	0.60	2854	35692.0	0.73	700.0	6461.0	42153.0
TMS [47]	0.31	3633	23531.0	0.50	891.0	5663.0	29194.0
CCMPA [48]	1.36	4411	124623	1.36	1082	18657	143279
TEC [49]	0.66	1038	14361.0	0.80	254.0	2600.0	16960.0
Turgay et al. [50]	0.71	4411	65569.0	0.80	1082	11053	76622.0

The best approximation for the stiffness of the simplified formulas to the behavior of the infilled frame ($k_{strut\ model}$) is the one whose ratio $k_{strut-mode}\ /k_{strut-tes}$ is close to unity, where k_{strut} = 126,400 kN/m, in order to accurately reproduce the initial stiffness of the infilled frame in its first cycles. The results of this ratio are shown in Figure 17.

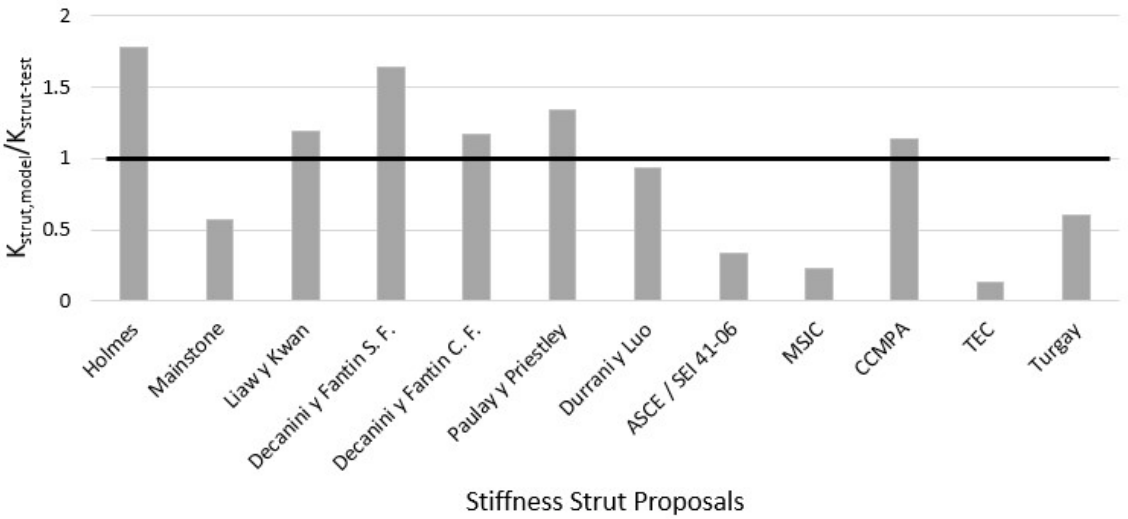

Figure 17. Ratios of model-to-test strut stiffness: $k_{\_(strut\text{-}model)}/k_{\_strut\text{-}test}$ for infilled frame.

In view of the results obtained, the formulations that are closest to the stiffness of the infill are those proposed by Durrani and Luo (1994) [45] and by CCMPA (2009) [48]. Both would be good choices for modeling the façade infill taking into account all the uncertainties involved. It was decided to use the formulation proposed by the Canadian CCMPA (2009) [48], because authors preferred to overestimate the stiffness in order to better prevent brittle failures and because it is a comprehensive guide on seismic design.

5. SEISMIC ASSESSMENT OF A RESIDENTIAL BUILDING IN LORCA (MURCIA, SPAIN)

On May 11, 2011 at 6:47 p.m., an M5.1 earthquake took place in Lorca at a depth of 4 km, registering 0.37g PGA, more than twice the seismic map PGA prescribed in the Standard. The catastrophe caused by the 2011 Lorca earthquake (Murcia, Spain) led to damage both in terms of human lives and buildings. Approximately 80% of the residential buildings were affected to various degrees of damage, 5% with severe structural damage and 13% with moderate structural damage, in addition to the damage of infrastructure and public buildings. Some of the structural failures and damage occurred in buildings that, somehow, had seismic considerations in their design. The seismic assessment of an actual apartment building in Lorca was conducted with the aim of explaining the reason for this result. The building was designed according to the current standard practice by industry professionals, which means without considering the masonry infills as structural elements. The seismic assessment included, in a simplified way, the effect of the infills in the façade walls. The equivalent stiffness contributions of the walls was calculated as shown in Section 4.2, calibrated with the experimental results and introduced into the numerical model as diagonal struts. In this way the global stiffness of the building is more realistic, and a modal spectral analysis is carried out obtaining modal displacements and shear forces on columns. A section level analysis is conducted to check columns' section capacity versus demand.

5.1 Building Description

The building under study is a typical residential apartment building in the city of Lorca (Murcia, Spain) that represents many buildings in other cities located in active seismic areas. The building consists of six floors (one ground floor and five floors of apartment) plus a penthouse. The footprint of the building is 28.79 m by 9.20 m. The floor height is 3 m, which gives a total building height of 21.40 m (Figure 18).

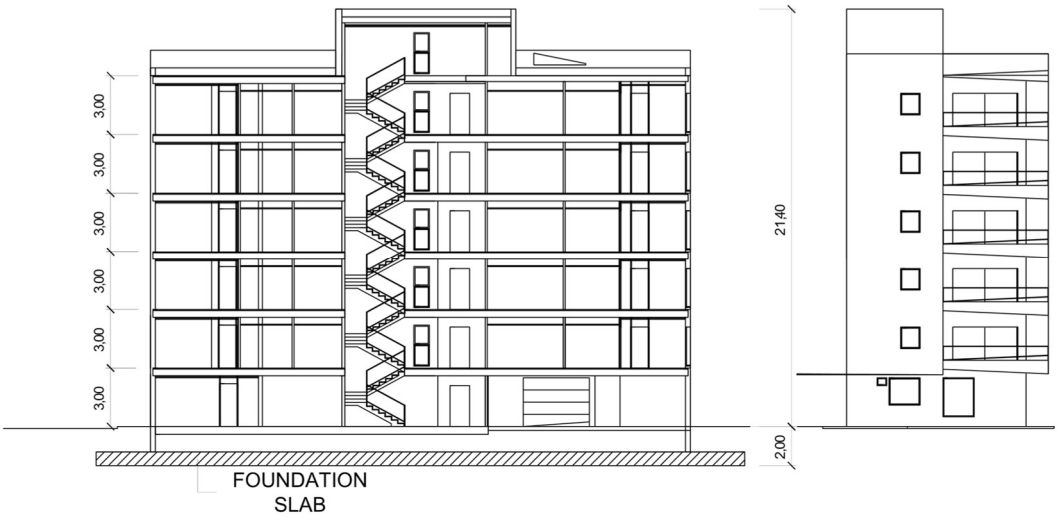

Figure 18. Elevation and side views of the apartment building

The shallow foundation comprised a continuous reinforced concrete mat of 0.7 m thickness and 33.24x13.64 m footprint founded at 2 m depth and made with 30 MPa compressive strength reinforced concrete. At ground level, a sanitary slab is designed with the same plan dimensions as the building and is 0.40 thick.

The lateral load resisting system of the building is composed of reinforced concrete frame with compressive strength of 30 MPa in the columns and 25 MPa in the beams. The building satisfied all the requirements of the Spanish Seismic Standard according to its seismic design acceleration, aiming at the philosophy 'strong-column weak beam'. The cross section of the columns is variable, decreasing with height. The largest section of the columns is 500x500 mm and the smallest is 300x300 mm. A plan view of the column layout is shown in Figure 19 and the cross sections can be found in Figure 24.

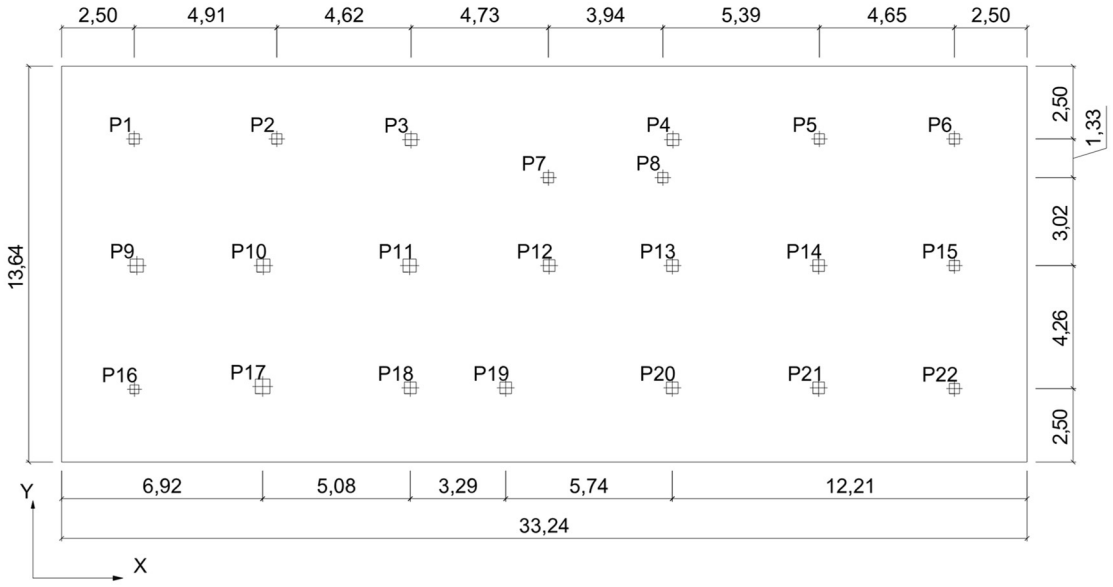

Figure 19. Plan view of the column distribution

The waffle floor slabs have a total thickness of 350 mm including 50 mm thick topping concrete solid slab and embedded wide beams of 350 mm total thickness and 200 to 550 mm width. One

of the corners of the building has a 150 mm solid slab system supported on beams, as highlighted in Figure 20. Every floor has a cantilever balcony of 4.5 m span in one corner of the building from floor 1 to 7.

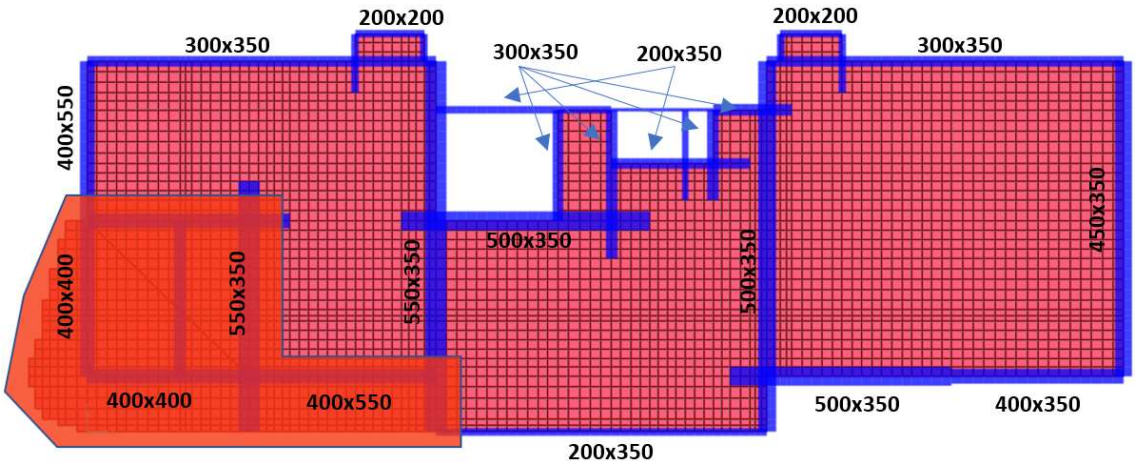

Figure 20. Building floor slab: solid slab area highlighted in the plan view, beam cross section dimensions shown.

The roof of the building is solved with a one-way slab, formed by prestressed joists and vaults. The concrete strength of the slabs and vaults is 25 MPa, while those of the joists is 45 MPa. The reinforcing steel used throughout the structure is B-500-S type (500 MPa yield strength) while the prestressing wires of the joists are Y1860C (1860 MPa tensile strength).

The façade infill panel has the same characteristics as used in the experimental phase: two brick layers (an exterior perforated brick layer and an interior hollow brick layer) bonded with ordinary mortar M7.5.

5.2 Loads

Three Standards were used to determine the loads acting on the structure [39], [40], [41]. The gravity loads include self-weight of structural elements, superimposed dead loads and live loads. The estimated dead load in each floor is 2 kN/m^2. The CTE-DB-SE-AE [51] establishes that the live load for apartment buildings is 2 kN/m^2.

The seismic forces were established in two orthogonal plan directions (X and Y) and their responses combined according to Seismic Standard NCSE-02 [28] clause 3.4. The current building configuration exempts it from vertical earthquake force considerations (Section 4.3.3.5.2 Eurocode 8 [52]). Based on the Spanish Standard, seismic analysis was performed using response spectrum modal analysis. The normalized inelastic response spectrum (α(T), ratio between spectral acceleration and peak ground acceleration, PGA) proposed by the NCSE-02 Standard for Lorca (affected by the ductility factor μ=2 and 5% of damping ratio) is depicted in Figure 21. It will be multiplied by the PGA for design, which is 0.156g.

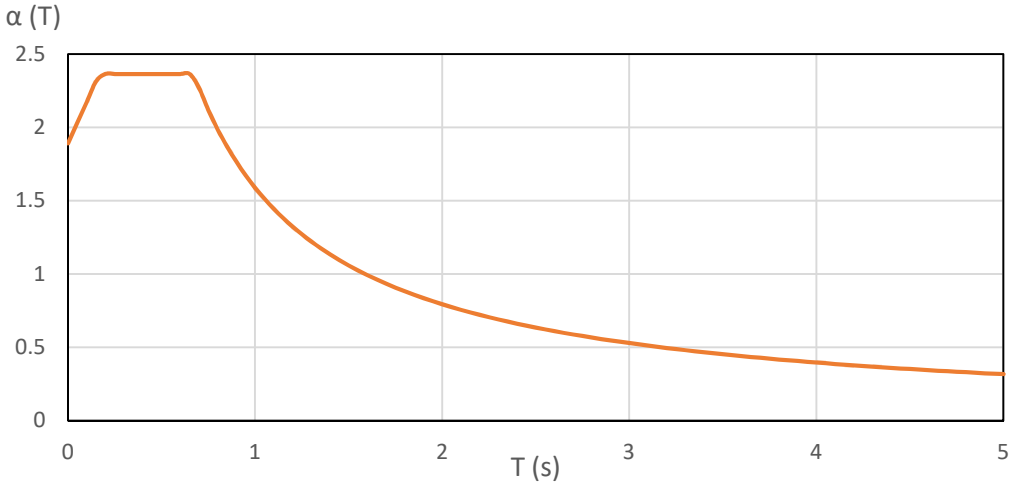

Figure 21. Normalized inelastic response spectrum for Lorca (Spain) (ductility factor μ=2, damping ratio 5%)

According to EC-8 [52], the seismic mass was considered as dead load mass plus 50% of the live load in the case of residential buildings, and 50 modes of vibration were taken into account resulting with an effective modal mass participation higher than 90% of the total mass of the structure.

5.3 Numerical Model Description

To account for the effect of non-structural infills in the design of the structure, the following models were built:

- Model 1: In this model the entire building is represented without modeling the façade masonry infills and is used for the seismic design of the building as in routine practice.
- Model 2: Similar to Model 1, except that it includes the modeling of the façade infills (see Figure 22), which have the same configuration as the masonry infill used in the infilled frame specimen. This model will be used for the seismic assessment of the 'as built' building considering struts in one direction and repeated considering the struts in the opposite direction. For every façade panel, the sum of the stiffnesses of both layers making up the façade provides the elastic stiffness of the springs to be used in model:

$$k_{facade\ strut} = \sum k_{layer\ strut} \quad \text{with} \quad k_{layer\ strut} = \frac{E_w \cdot A_w}{d} \qquad A_w = w \cdot t_w$$

where:

$k_{layer\ strut}$	Stiffness of a spring that represents one layer of the masonry infill
E_w	Modulus of elasticity for the equivalent strut
A_w	Equivalent diagonal strut cross-sectional area
w	Equivalent diagonal strut width
t_w	Brick layer thickness
d	Frame diagonal Length

As discussed earlier, the parameters d and t_w are known, so to obtain the two missing parameters (strut width and modulus of elasticity) the formulation of the Canadian CCMPA standard is used, in accordance with Section 4 of this paper. The formulas used from the CCMPA method are:

$$E_w = 850\, f_k$$

$$w \leq \begin{cases} w_e/2 \\ d/4 \end{cases} \qquad w_e = \sqrt{\alpha_h^2 + \alpha_L^2}$$

$$\alpha_h = \frac{\pi}{2} \sqrt[4]{\frac{4E_c I_c H}{E_w t_w \sin 2\theta}} \qquad \alpha_L = \pi \sqrt[4]{\frac{4E_c I_v H}{E_w t_w \sin 2\theta}}$$

where:

f_k	Masonry characteristic compressive strength, in MPa
E_c	Modulus of elasticity of the column
I_c	Moment of inertia of the column
I_v	Moment of inertia of the beam
H	Horizontal length of the masonry panel
θ	Angle between the diagonal strut and the horizontal line

The value of the characteristic compressive strength of the masonry is obtained from the formulation proposed by Eurocode 6 [53] in section 3.6.1.2:

$$f_k = K\, f_b^{0.7}\, f_m^{0.3}$$

where:

K	Constant that depends on the type of mortar and brick, extracted from Table 3.3 of the aforementioned Eurocode.
f_b	Average normalized compressive strength for the bricks, in MPa.
f_m	Compressive strength of mortar, in MPa.

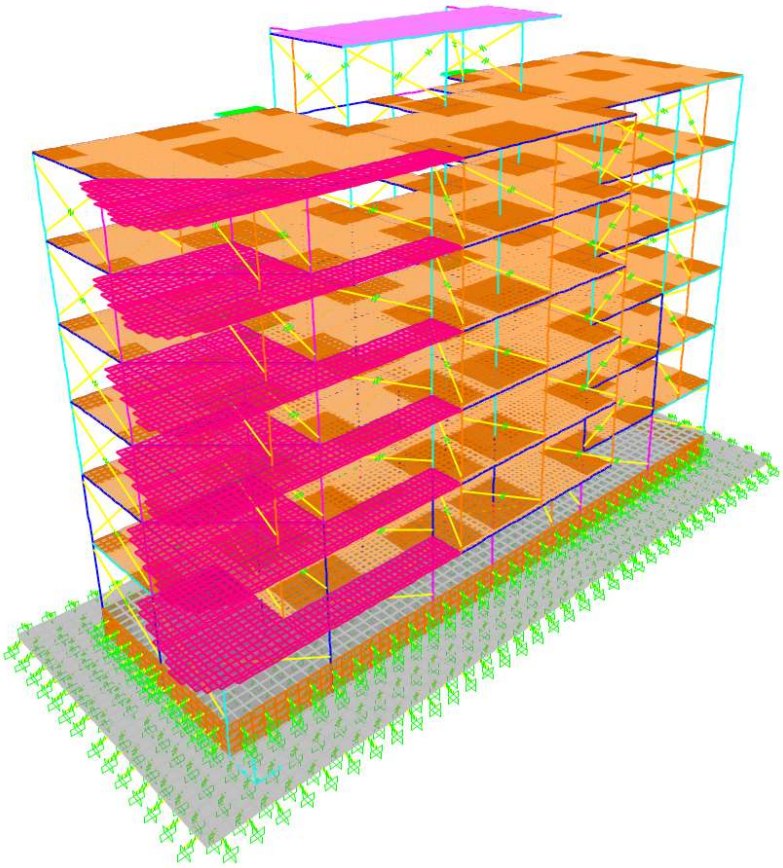

Figure 22. Numerical model of the building including diagonal struts for façade enclosure.

5.4 Modes of vibration

In the modal analysis of Model 1, the fundamental period is 0.95 s corresponding to the first mode shape in Y-direction (Table 6). In Model 2, with the inclusion of façade masonry infills, the first mode shape remained in the Y-direction, however, its period was reduced to 0.69 s (Table 7). This represents almost a 30% reduction, which is a considerable increase in the stiffness of the building provided by the façade infill. This decrease in the period entails a considerable 42% increase in the pseudo-acceleration ($\alpha(T)$) from 1.67 (Model 1) to 2.37 (Model 2) moving from the seismic force decay branch to the plateau, as shown in Figure 23, with the consequent increase in the seismic force.

Table 6. Modal characteristics of Model 1.

			Modal effective masses					
	#	**Period (s)**	**D_X**	**D_Y**	**D_Z**	**R_X**	**R_Y**	**R_Z**
Modes	1	0.947	0.06350	0.68560	7.175E-05	0.15905	0.00584	0.02857
	2	0.920	0.71525	0.06959	2.325E-07	0.01501	0.05910	0.00111
	3	0.855	0.00606	0.02379	2.490E-05	0.00545	0.00135	0.76535
	4	0.324	0.02639	0.08327	2.600E-04	0.28203	0.03877	0.00837
	5	0.318	0.08461	0.02593	1.211E-05	0.09153	0.12114	0.00143
	6	0.288	0.00025	0.00838	0.000310	0.03580	0.00145	0.10177

Table 7. Modal characteristics of Model 2.

			Modal effective masses

	#	Period (s)	D_X	D_X	D_X	D_X	D_X	RZ
Modes	1	0.688	0.00038	0.78945	0.00024	0.17726	5.959E-05	3.172E-05
	2	0.480	0.42084	0.00041	0.00012	0.00001	0.02945	0.39413
	3	0.446	0.40632	0.00057	1.052E-06	0.00075	0.03365	0.41953
	4	0.225	0.00206	0.12595	0.00155	0.46640	0.00079	1.172E-06
	5	0.161	0.06839	0.00083	0.00086	0.00096	0.16306	0.03792
	6	0.155	0.02825	0.00079	0.01188	0.00034	0.14010	0.06367

5.5 Seismic assessment and influence of the masonry infills

According to Álvarez et al. (2013) [54], the role the non-structural elements played in the damage observed after the 2011 Lorca earthquake was fundamental. Many columns experienced shear cracks concentrated in a length of around 500-600 mm below or above beam level due to the concentrated forces exerted by the diagonal struts on these sections along with captive column effects. This fact is also observed in Figure 13c with 600 mm of crushed infill in the column's contact. An offset of 300 mm from the columns' joints to account for the diagonal compression effect better reflects the location of the thrust exerted by the strut. This is a simplification of some of the multi-strut macromodels proposed by authors like Crisafulli and Carr [55], in line with the proposals of standards and manuals, such as ASCE/SEI 41-06 [56] and FEMA [57] using a single off-diagonal strut with a fixed location. In this sub-section, column failure will become evident when structurally assessing the sections under the influence of masonry infills.

There are 134 columns in the building (see Figure 23), each of them divided into 10 elements in the model. The two elements at column top and bottom of every column have been checked for normal and shear stresses in Model 2 when considering the façade enclosure hypothesis, leading to 536 elements checked.

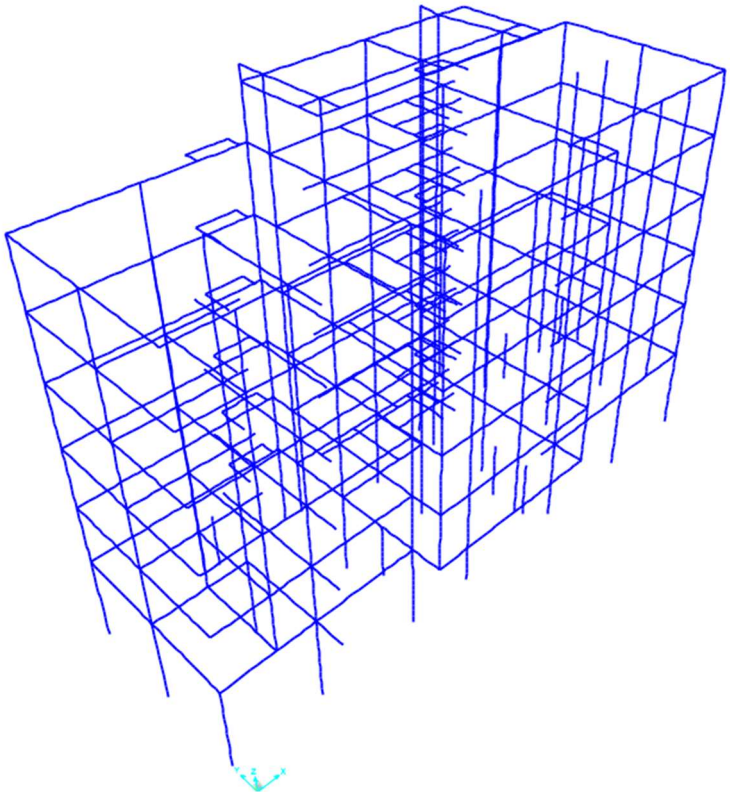

Figure 23. 3D view of the column layout

The shear-wall effect created by the façade infill decreases the displacements in the model, reducing the bending failure in columns. However, shear forces induced in the columns by the struts led to shear failure at column ends, as shown in Figure 25, where the failed elements are shaded. The columns presenting a few failed elements is because they do not have façade panels, mainly being interior columns, as can be seen in Figures 19 and 22.

		P1	P2	P3	P4	P5	P6	P7	P8	P9	P10	P11	P12	P13	P14	P15	P16	P17	P18	P19	P20	P21	P22
FROM 6 TO 7	ϕ_stirrup (mm)			6	6			6	6			6	6	6									
	s_stirrup (cm)			10	10			10	10			10	10	10									
	b (cm)			30	30			30	30			30	30	30									
	h (cm)			30	30			30	30			30	30	30									
FROM 5 TO 6	ϕ_stirrup (mm)	6	6	6	6	6	6	6	6	6	6	6	6	6	6	6		6	6	6	6	6	6
	s_stirrup (cm)	10	10	10	10	10	10	10	10	10	10	10	10	10	10	10		10	10	10	10	10	10
	b (cm)	30	30	30	30	30	30	30	30	40	40	30	30	30	30	30		40	30	30	30	30	30
	h (cm)	30	30	30	30	30	30	30	30	40	40	30	30	30	30	30		40	30	30	30	30	30
FROM 4 TO 5	ϕ_stirrup (mm)	6	6	6	6	6	6	6	6	6	6	6	6	6	6	6		6	6	6	6	6	6
	s_stirrup (cm)	10	10	10	10	10	10	10	10	10	10	10	10	10	10	10		10	10	10	10	10	10
	b (cm)	30	30	30	30	30	30	30	30	40	40	35	30	30	30	30		40	30	30	30	30	30
	h (cm)	30	30	30	30	30	30	30	30	40	40	35	30	30	30	30		40	30	30	30	30	30
FROM 3 TO 4	ϕ_stirrup (mm)	6	6	6	6	6	6	6	6	6	6	6	6	6	6	6		6	6	6	6	6	6
	s_stirrup (cm)	10	10	10	10	10	10	10	10	10	10	20	10	10	10	10		10	10	10	10	10	10
	b (cm)	30	30	30	30	30	30	30	30	40	40	35	30	30	35	30		40	30	30	30	30	30
	h (cm)	30	30	30	30	30	30	30	30	40	40	35	30	30	35	30		40	30	30	30	30	30
FROM 2 TO 3	ϕ_stirrup (mm)	6	6	6	6	6	6	6	6	6	6	6	6	6	6	6		6	6	6	6	6	6
	s_stirrup (cm)	10	10	10	10	10	10	10	10	10	10	10	10	10	10	10		10	10	10	10	10	10
	b (cm)	30	35	30	30	30	30	30	35	40	40	35	30	35	35	30		40	30	30	30	35	30
	h (cm)	30	35	30	30	30	30	30	35	40	40	35	30	35	35	30		40	30	30	30	35	30
FROM 1 TO 2	ϕ_stirrup (mm)	6	6	6	6	6	6	6	6	6	6	6	6	6	6	6		6	6	6	6	6	6
	s_stirrup (cm)	10	10	10	10	10	10	10	20	10	10	10	10	10	10	10		10	10	10	10	10	10
	b (cm)	35	35	35	35	35	30	35	35	40	40	40	35	35	35	35		45	35	35	35	35	30
	h (cm)	35	35	35	35	35	30	35	35	40	40	40	35	35	35	35		45	35	35	35	35	30
FROM 0 TO 1	ϕ_stirrup (mm)	6	6	6	6	6	6	6	6	6	6	6	6	6	6	6	6	6	6	6	6	6	6
	s_stirrup (cm)	10	10	10	10	10	10	10	10	10	10	10	10	10	10	10	10	10	10	10	10	10	10
	b (cm)	35	35	40	40	35	35	35	35	45	45	45	40	40	40	35	30	50	40	40	40	40	35
	h (cm)	35	35	40	40	35	35	35	35	45	45	45	40	40	40	35	30	50	40	40	40	40	35

Figure 25. Cross section, column hoops and shear failure of columns

Therefore, even with the fact that the building was designed with seismic provisions, the consideration of the stiffness provided by the infills and the effect of the diagonal struts increase the failure of column ends by shear, which would require an increase in the transverse reinforcement or column cross sections to avoid this brittle failure. As commented, it is important to point out here that many buildings after the Lorca earthquake shown shear failures in many columns of masonry infilled frames, which is in line with the results obtained here. Table 8 shows the ratio between columns' shear force in model 2 vs model 1 (V_{model2}/V_{model1}), with large variations depending on the floor and the column. For the studied case, as a rule of thumb, the average increase in the columns' shear force per floor considering the infill contribution can be estimated as twice the value without considering the infills.

Table 8. Columns' shear force ratio between model 2 and model 1

																								AVERAGE	
FROM 6 TO 7			0.33	5.39			1.38	0.48			2.65	2.16	1.77										2.02	
FROM 5 TO 6	4.64	2.27	2.58	4.17	3.20	3.51	4.21	0.68	1.85	0.75	0.86	0.78	0.66	0.54	2.04		1.11	2.56	0.81	1.62	4.32	0.73	2.09	
FROM 4 TO 5	3.14	2.72	2.26	4.20	3.06	5.00	3.79	0.58	3.01	0.68	0.77	0.68	0.59	0.49	1.46		0.90	2.98	0.69	1.42	4.10	0.60	2.05	
FROM 3 TO 4	3.07	3.15	2.25	4.28	2.99	5.55	3.99	0.56	3.08	0.65	0.75	0.66	0.59	0.50	1.39		0.82	3.24	0.59	1.31	4.27	0.58	2.11	2.16
FROM 2 TO 3	3.31	2.18	2.44	4.77	3.23	6.45	4.96	0.57	3.14	0.65	0.75	0.66	0.62	0.53	1.53		0.84	3.69	0.52	1.30	2.74	0.58	2.16	
FROM 1 TO 2	2.69	2.65	1.84	3.68	2.13	8.73	4.08	0.62	4.05	0.67	0.73	0.69	0.69	0.61	1.16		0.86	2.80	0.49	1.11	3.52	0.55	2.11	
FROM 0 TO 1	4.87	2.08	0.75	0.78	0.75	0.58	5.13	2.21	2.64	0.74	0.81	0.84	0.81	0.74	5.21	10.03	1.59	2.72	0.66	1.12	2.96	6.36	2.47	
	P1	P2	P3	P4	P5	P6	P7	P8	P9	P10	P11	P12	P13	P14	P15	P16	P17	P18	P19	P20	P21	P22		

6. CONCLUSIONS

The current study presented an experimental and analytical investigation of the effect of the inclusion of masonry infill façade panels on the seismic response of concrete frames. The following conclusions can be drawn based on the experimental results and the comparison of the equivalent strut macro-models:

- The behavior of the bare frame is 'relatively' elastic in low amplitude drift cycles with narrow hysteresis loops. The behavior of the masonry infilled frame is also somewhat elastic in the first two cycles, but wider hysteresis loops appear after the

third one becoming soon nonlinear. The force-deformation curve features two peaks: the first corresponds to the onset of degradation of the infill due to the formation of diagonal compression struts along with frame member cracking, followed by a drop in the lateral force capacity. With increasing drift amplitudes, the lateral force increases again, reaching a lower second peak. The initial failure mode evolves into a failure mode similar to the flexural-shear mode observed in the bare frame, which is yielding of the longitudinal steel and concrete cracking at beam and column ends, forming plastic hinges along with shear cracking. The contribution of the secondary struts results in a higher final strength.

- Considering façade masonry infill in a concrete frame resulted in eight times stiffness increase compared to the bare frame-for a scheme similar to the one tested in this study.
- Basic dynamic parameters such as stiffness and fundamental period of the bare frame are very well captured by the model, with an error of 1.9% in initial stiffness estimation.
- Among the 12 mathematical strut macro-models studied, the models that best predicted the stiffness of the masonry infills when modeling with diagonal struts are the ones by Durrani and Luo (1994) [45] and the Canadian Seismic Standard CCMPA [48]. The latter was adopted in order to conservatively estimate the stiffness to better prevent brittle failures.

The seismic response of building numerical models when considering façade masonry infills in the form of equivalent diagonal struts in a 7-story residential building representative of the city of Lorca was investigated in the current study, yielding the following conclusions.

- The consideration of masonry infills in building concrete frames significantly increases the stiffness of the structure, decreases the fundamental periods and increases seismic forces. In the building studied, the fundamental period reduction was approximately 30%, moving the initial seismic spectral accelerations to the plateau area in the response spectrum, increasing the seismic demand by about 80%.
- Masonry infills change the way that framed buildings resist bending and their overall structural behavior. Without the façade partitions, bending in columns and beams is the main resisting mechanism. When considering the infills in the models, the bending is resisted by buildings as: a) shear wall effect appears in the panels, b) infill struts exert at the column top and bottom increasing shear stresses, that are proportional to the panel stiffness, and c) brittle shear failure in columns is more likely.

The proposed infill modeling procedure easily allows structural engineers to consider in their models different hypotheses, even taking into account the presence or absence of the interior partitions of the buildings, thus covering a wider range of possible seismic responses and situations during the lifetime of a building, allowing more informed and realistic bounding analysis and increasing the safety of seismic design. The reader is aware that response under in plane drifts is an interactive process because out-of-plane effects occur simultaneously, leading to an increase in the vulnerability of infill walls. Proper consideration needs to be given to this fact to improve the overall behavior.

7. ACKNOWLEDGMENTS

The present study was supported by the Universitat Politècnica de València (UPV) and the Spanish Ministry of Economy and Competitiveness through Project BIA2015-70651-R, the Ministry of Science, Innovation and Universities through Project FPU16/0354, and Generalitat Valenciana (GVA) by BEST2018.

8. REFERENCES

[1] Federal Emergency Management Agency. (2009). Unreinforced Masonry Buildings and Earthquakes. Developing Successful Risk Reduction Programs. FEMA P-774 / October 2009.

[2] Smith B. S., Carter C. (1969). A method of analysis for infilled frames. *ICE Proc., N*ovember, 44(1), pp. 31-48.

[3] Bertero V., Brokken S. (1983). Infills in Seismic Resistant Building. *Journal of Structural Engineering,* Junio, 109(6), pp. 1337-1361.

[4] Negro P., Verzeletti G. (1996). Effect of Infills on the Global Behaviour of R/C Frames: Energy Considerations from Pseudodynamic Tests. *Earthquake Engineering and Structural Dynamics,* Febrero, Volumen 25, pp. 753-773.

[5] Al-Chaar G., Issa M., Sweeney S., (2002). Behavior of Masonry-Infilled Nonductile Reinforced Concrete Frames. *Journal of Structural Engineering,* Agosto, 128(8), pp. 1055-1063.

[6] El-Dakhakhni WW. (2002). Experimental and Analytical Seismic Evaluation of Concrete Masonry-Infilled Steel Frames Retrofitted using GFRP Laminates. PhD Thesis. Drexel University, Philadelphia, Pennsylvania, USA, 2002.

[7] Pallarés F.J., Pallarés L. (2016). Experimental study on the response of seismically isolated masonry infilled steel frames during the initial stages of a seismic movement. Engineering Structures 129 (2016) 44–53. http://dx.doi.org/10.1016/j.engstruct.2016.09.019.

[8] Ricci P, De Risi MT, Verderame GM, Manfredi G. (2013). Influence of infill distribution and design typology on seismic performance of low- and mid-rise RC buildings. Bull Earthq Eng 2013; 11 (5): 1585–616. http://dx.doi.org/10.1007/s10518-013-9453-4.

[9] Alarcón E, Benito M. (2014). Foreword special issue LORCA's earthquake. Bull. Earthq. Eng. 2014; 12 (1827): 2014. http://dx.doi.org/10.1007/s10518-014-9602-4.

[10] Gómez Martínez F. (2015). FAST simplified vulnerability approach for seismic assessment of infilled RC MRF buildings and its application to the 2011 Lorca (Spain) earthquake. Universitat Politècnica de València 2015. http://dx.doi.org/10.4995/Thesis/10251/54780.

[11] De Luca F, Verderame GM, Gomez-Martinez F, Perez-Garcia A. The structural role played by masonry infills on RC building performances after the 2011 Lorca, Spain, earthquake. Bull Earthq Eng 2014; 12 (5): 1999–2026. http://dx.doi.org/10.1007/s10518-013-9500-1.

[12] Hermanns L, Fraile A, Alarcón E, Álvarez R. (2014). Performance of buildings with masonry infill walls during the 2011 Lorca earthquake. Bull Earthq Eng 2014; 12 (5): 1977–97. http://dx.doi.org/10.1007/s10518-013-9499-3.

[13] Ruiz-Pinilla JG, Adam JM, Pérez-Cárcel R, Yuste J, Moragues JJ. (2016). Learning from RC building structures damaged by the earthquake in Lorca, Spain, in 2011. Eng Fail Anal 2016; 68. http://dx.doi.org/10.1016/j.engfailanal.2016.05.013.

[14] Romão X, Costa AA, Paupério E, Rodrigues H, Vicente R, Varum H, Costa A. (2013). Field observations and interpretation of the structural performance of constructions after the 11 May 2011 Lorca earthquake. Eng Fail Anal 2013; 34: 670–92. http://dx.doi.org/10.1016/j.engfailanal.2013.01.040.

[15] Laura Liberatore, Fabrizio Noto, Fabrizio Mollaioli, Paolo Franchin. In-plane response of masonry infill walls: Comprehensive experimentally-based equivalent strut model for deterministic and probabilistic analysis. Engineering Structures 167 (2018) 533–548. https://doi.org/10.1016/j.engstruct.2018.04.057

[16] Gergis, S., and Hassan, W. M. (2014). Macro-modeling for Seismic Shear Strength of Masonry Infilled Reinforced Concrete Frames. Proceedings, 10th U.S. National Conference on Earthquake Engineering, Earthquake Engineering Research Institute, July 21-25. Anchorage, Alaska.

[17] Sandoli, A., Musella, C., Lignola, G.P., Calderoni, B. and Prota, A. (2020) Spandrel panels in masonry buildings: Effectiveness of the diagonal strut model within the equivalent frame model. *Structures* 27, (2020) 879-893. https://doi.org/10.1016/j.istruc.2020.07.001

[18] Kareem K.M., Pantò B. (2019). Simplified macromodelling strategies for the seismic assessment of non-ductile infilled frames: a critical appraisal. *Journal of Building Engineering*, 22 (2019) 397-414. https://doi.org/10.1016/j.jobe.2018.12.010

[19] Huang, H. and Burton, H. (2019) Classification of in-plane failure modes for reinforced concrete frames with infills using machine learning. *Journal of Building Engineering,* 25 (2019). https://doi.org/10.1016/j.jobe.2019.100767

[20] J. Yu, Y.-P. Gan, J. Wu, and H. Wu, (2019). Effect of concrete masonry infill walls on progressive collapse performance of reinforced concrete infilled frames. Engineering Structures, vol. 191, pp. 179–193. https://doi.org/10.1016/j.engstruct.2019.04.048

[21] Stavridis A., Koutromanos, I, Shing P.B., (2012). Shake-table tests of a three-story reinforced concrete frame with masonry infill walls. Earthquake Engineering & Structural Dynamics, vol. 41, no. 6, pp. 1089–1108. https://doi.org/10.1002/eqe.1174

[22] Hashemi A., Mosalam K.M. (2006). Shake-table experiment on reinforced concrete structure containing masonry infill wall. Earthq. Eng. Struct. Dyn., 35 (14) (2006), pp. 1827-1852. https://doi.org/10.1002/eqe.612

[23] Costa Alexandre, Penna Andrea, Magenes Guido. (2011). Seismic Performance of Autoclaved Aerated Concrete (AAC) Masonry: From Experimental Testing of the In-Plane Capacity of Walls to Building Response Simulation. Journal of Earthquake Engineering. 15. 1-31. 10.1080/13632461003642413. https://doi.org/10.1080/13632461003642413

[24] Markulak D, Radic I, Sigmund V. (2013). Cyclic testing of single bay steel frames with various types of masonry infill. Engineering Structures. 51:267–77. https://doi.org/10.1016/j.engstruct.2013.01.026

[25] C. Zhai, J. Kong, X. Wang, Z. Chen. (2016). Experimental and finite element analytical investigation of seismic behavior of full-scale masonry infilled RC frames. J. Earthq. Eng., 20 (7), pp. 1171-1198. https://doi.org/10.1080/13632469.2016.1138171

[26] V. Palieraki, C. Zeris, E. Vintzileou, and C.-E. Adami. (2018). In-plane and out-of plane response of currently constructed masonry infills. Engineering Structures, vol. 177, pp. 103–116. https://doi.org/10.1016/j.engstruct.2018.09.047

[27] R. Furtado, H. Rodrigues, A. Arêde, H. Varum. (2018). Double-leaf infill masonry walls cyclic in-plane behaviour: experimental and numerical investigation. Open Construct Build Technol J. 2018;12:35–48. DOI: 10.2174/1874836801812010035.

[28] NCSE-02. (2002) Seismic-resistant Construction Standard: general part and building (NCSE-02). Ministerio de Fomento.

[29] EHE-08 (2010). Instrucción de hormigón estructural. Madrid. Ministerio de Fomento, Comisión Per manente del Hormigón. 2010.

[30] UNE EN 12390-1:2013. (2013). Testing hardened concrete - Part 1: Shape, dimensions and other requirements for specimens and moulds. European Standards.

[31] UNE EN 1015-11. (2020) Methods of test for mortar for masonry - Part 11: Determination of flexural and compressive strength of hardened mortar. European Standards.

[32] *UNE-EN 771-1:2011+A1* Materiales cerámicos de arcilla cocida para la construcción. (2016). *Especificaciones de piezas para fábrica de albañilería. Parte 1: Piezas de arcilla cocida.* Bruselas, Bélgica: AENOR.

[33] FEMA. (2007). *Interim Testing Protocols for Determining the Seismic Performance Characteristics of Structural and Nonstructural Components Through Laboratory Testing - FEMA - 461.* Federal Emergency Management Agency Washington, DC. 2007.

[34] Tall Buildings Initiative (TBI). (2017). "Guidelines for Performance-Based Seismic Design of Tall Buildings". Pacific Earthquake Engineering Research Center. PEER Report No. 2017/06. Version 2.03.

[35] Hassan, W. M., "Analytical and Experimental Assessment of Seismic Vulnerability of Beam-Column Joints without Transverse Reinforcement in Concrete Buildings," PhD Dissertation, University of California, Berkeley, CA, May 2011. https://escholarship.org/uc/item/1k49h3mx

[36] Hassan, W. M., and Moehle, J. (2012). Experimental Assessment of Seismic Vulnerability of Corner Beam-Column Joints in Older Concrete Buildings. Proceedings, 15th World Conference on Earthquake Engineering, Lisbon, Portugal.

[37] Hassan, W. M. and Moehle, J. P., "Shear Strength of Exterior and Corner Beam-Column Joints without Transverse Reinforcement," ACI Structural Journal, Vol. 115, No. 6, Nov 2018, pp. 1719-1727. DOI: https://doi.org/10.14359/51702416

[38] CSI, Inc. (2013). SAP2000 v16.1.1. Integrated finite element analysis and design of structures. Computers and Structures Inc., Berkeley (CA, USA).

[39] Eurocode 2. (2013). *Eurocode 2: Design of concrete structures - Part 1: General rules and rules for buildings.* Brussels, Belgium.

[40] Holmes, M. (1961). Steel frames with brickwork and concrete infilling. *ICE Proc.,* October, 19(4), pp. 473-478.

[41] Mainstone, R. J. (1971). On the stiffness and strengths of infilled frames. *ICE Suppl.,* Volumen 4, pp. 57-90.

[42] Liauw, T. C. & Kwan, K. H. (1985). Unified Plastic Analysis for Infilled Frames. *Journal of Structural Engineering,* Julio, 111(7), pp. 1427-1448.

[43] Decanini, L. D. & Fantin, G. E. (1987). *Modelos simplificados de la mampostería incluida en pórticos. Características de rigidez y resistencia lateral en estado límite.* Buenos Aires, Argentina, pp. 817-836.

[44] Paulay, T. & Pristley, M. J. N. (1992). *Seismic design of reinforced concrete and masonry buildings,* New York: A Wiley Interscience Publication.

[45] Durrani, A. J. & Luo, Y. H. (1994). *Seismic retrofit of flat-slab buildings with masonry infills,* Buffalo, New York: National Center for Earthquake Engineering Research (NCEER).

[46] ASCE/SEI. (2007). *Standard 41-06: Seismic Rehabilitation of Existing Structures. ASCE 2007.* Reston, Virginia, USA.

[47] TMS 402/602-16 Building Code Requirements and Specification for Masonry Structures. (2016). *Building code requirements and specification for masonry structures.* The Masonry Society, CO USA.

[48] CCMPA. (2009). *Seismic design guide for masonry buildings.* Canadian Concrete Masonry Producers Association. Toronto, Canada.

[49] TEC. (2007). *Turkish Code for Buildings in Seismic Zones.* The Ministry of Public Works and Settlements. Ankara, Turkey.

[50] Turgay, T., Durmus, M. C., Binici, B. & Ozcebe, G. (2014). Evaluation of the Predictive Models for Stiffness, Strength, and Deformation Capacity of RC Frames with Masonry Infill Walls. *Journal of Structural Engineering,* May, pp. 1-9.

[51] CTE-DB-SE-AE. (2009). *Documento Básico de Seguridad Estructural. Acciones en la edificación.* Ministerio de Fomento, Madrid, España.

[52] UNE-EN 1998-1. (1998). *Eurocode 8: Design of structures for earthquake resistance. Part 1: General rules, seismic actions and rules for buildings.*

[53] UNE-EN 1996-1-2. (2013). *Eurocode 6: Design of masonry structures -Part 1-1: General rules for reinforced and unreinforced masonry structures.*

[54] Álvarez R., Díaz-Pavón E., Rodríguez R. (2013). El terremoto de Lorca. Efectos en los edificios. Consorcio de Compensación de Seguros. Ministerio de Economía y Competitividad.

[55] Crisafulli F.J., Carr A.J. (2007). Proposed macro-model for the analysis of infilled frame structures. Bulletin of the New Zealand Society for Earthquake Engineering, Vol. 40, No. 2, June 2007. https://doi.org/10.5459/bnzsee.40.2.69-77.

[56] ASCE/SEI 41-06. ASCE/SEI 41-06 Seismic rehabilitation of existing buildings; 2007.

[57] Applied Technology Council (ATC-43 Project). FEMA 307 evaluation of earthquake damaged concrete and masonry wall buildings; 1998.